THE ASTROPHYSICAL JOURNAL, 467:19–37, 1996 August 10

GALAXY PAIRWISE VELOCITY DISTRIBUTIONS ON NONLINEAR SCALES

ANTONALDO DIAFERIO AND MARGARET J. GELLER
Harvard-Smithsonian Center for Astrophysics, 60 Garden Street, Cambridge, MA 02138;
adiaferio@cfa.harvard.edu; mgeller@cfa.harvard.edu.
Received 1995 November 8; accepted 1996 February 26

ABSTRACT

The redshift-space correlation function ξ_s for projected galaxy separations $\lesssim 1\ h^{-1}$ Mpc can be expressed as the convolution of the real-space correlation function with the galaxy pairwise velocity distribution function (PVDF). An exponential PVDF yields the best fit to the ξ_s measured from galaxy samples of different redshift surveys. We show that this exponential PVDF is not merely a fitting function but arises from well-defined gravitational processes. Two ingredients conspire to yield a PVDF with a nearly exponential shape: (1) the number density $n(\sigma)$ of systems with velocity dispersion σ and (2) the unrelaxed dynamical state of most galaxy systems. The former ingredient determines the exponential tail, and the latter determines the central peak of the PVDF.

We examine a third issue: the transfer of orbital kinetic energy to galaxy internal degrees of freedom. Although this effect is of secondary importance for the PVDF exponential shape, it is detectable in galaxy groups, which indicates that galaxy merging is an ongoing process in the present universe.

We compare the ξ_s measured on nonlinear scales from galaxy samples of the Center for Astrophysics redshift surveys with different models of the PVDF convolved with the measured real-space correlation function. This preliminary comparison indicates that the agreement between model and observations depends strongly on both the underlying cosmological model and the internal dynamics of galaxy systems. Neither parameter dominates. Moreover, the agreement depends sensitively on the accuracy of the galaxy position and velocity measurements.

We expect that ξ_s will pose further constraints on the model of the universe and will improve the knowledge of the dynamics of galaxy systems on very small scales if we improve (1) the galaxy coordinate determination and (2) the measurement of relative velocities of galaxies with small projected separation. In fact, the redshift-space correlation function ξ_s depends sensitively on the internal pairwise velocity distribution of individual galaxy systems for projected pair separations $\lesssim 0.5\ h^{-1}$ Mpc and relative velocities $\pi \lesssim 300$ km s^{-1}.

Subject headings: cosmology: theory — galaxies: distances and redshifts — galaxies: interactions — galaxies: kinematics and dynamics

1. INTRODUCTION

The pairwise velocity distribution function (PVDF) of galaxy systems has been studied since Geller & Peebles (1973) first used it to determine the mean mass of galaxy groups statistically. The PVDF assumed clear importance in cosmology when Peebles (1976) used it to determine the pairwise velocity dispersion $\sigma_{12}(r)$ of galaxy pairs separated by a projected distance $r \lesssim 1\ h^{-1}$ Mpc[1] and ultimately to determine the mean mass density of the universe.

Davis & Peebles (1983) first computed the redshift-space correlation function ξ_s as a convolution of the real space two-point correlation function with the galaxy PVDF. Recently, Fisher et al. (1994b) and Marzke et al. (1995) used the same "convolution method" to determine ξ_s and the pairwise velocity dispersion $\sigma_{12}(r)$ on nonlinear scales. All of this work, starting from Peebles (1976), assumes an exponential PVDF. Bean et al. (1983), Fisher et al. (1994b), and Marzke et al. (1995) demonstrate quantitatively that this shape fits the observations better than other distributions. However, so far the exponential shape has been a fitting function without any physical justification.

It is not clear what PVDF we should expect on nonlinear scales where nonlinear gravitational clustering erases information about the initial conditions. On linear scales ($r \gtrsim 10\ h^{-1}$ Mpc), if the standard inflationary model is valid, we expect a Gaussian PVDF (see, e.g., Nusser, Dekel, & Yahil 1995). As a two-point distribution, the PVDF is a more powerful tool than one-point distributions to determine whether the density fluctuations are Gaussian or non-Gaussian (see, e.g., Kofman et al. 1994; Catelan & Scherrer 1995). If the PVDF is indeed Gaussian on linear scales, we need a link between the observed exponential PVDF on nonlinear scales and the expected Gaussian in the linear regime (Fisher 1995).

Numerical work devotes attention mainly to the pairwise velocity dispersion $\sigma_{12}(r)$ rather than to the shape of the PVDF (see, e.g., Couchman & Carlberg 1992; Gelb & Bertschinger 1994). Efstathiou et al. (1988) simulate a flat universe with scale-free initial conditions; by analyzing the particle velocity field, they find a skewed PVDF with exponential tails but a flatter core at small relative velocities. Cen & Ostriker (1993) implicitly find the same result by simulating a standard CDM universe including dissipative galaxy formation. Their single-galaxy peculiar velocity exponential distribution implies a PVDF similar to the one found by Efstathiou et al. (Marzke et al. 1995). A variety of CDM models (Fisher et al. 1994b) confirm this behavior. All of this work has a dynamic range of roughly 3 orders of magnitude. With an order of magnitude increase in dynamic range, Zurek et al. (1994) study the massive halo

[1] $H_0 = 100\ h$ km s^{-1} Mpc^{-1} is the present Hubble constant, and we use $h = 0.5$ throughout.

velocity field and find an exponential skewed PVDF at all projected separations between 0.5 h^{-1} Mpc and 5.5 h^{-1} Mpc and for all relative velocities, which indicates that the flat core of previous simulations probably arose from an inadequate treatment of gravitational interactions on small scales.

All previous work, both observational and numerical, does not explain the physical origin of the exponential shape of the PVDF. Here we propose a simple physical argument for the observed exponential PVDF for galaxy separations $\lesssim 1\ h^{-1}$ Mpc.

If $n(\sigma)$ is the number density of galaxy systems with velocity dispersion σ, we show that the exponential tail can be obtained from the integral of Gaussian internal velocity distributions for each galaxy system weighted either with the observed $n(\sigma)$ or with the $n(\sigma)$ predicted by the Press & Schechter (1974) theory (§ 2).

Section 3 shows that the central peak of the PVDF requires the presence of unrelaxed systems with a non-Gaussian internal velocity distribution. In § 4 we examine a further process that can peak up the PVDF at small relative velocities: the transfer of orbital kinetic energy to galaxy internal degrees of freedom. In § 5 we compare various models of the PVDF with the redshift-space correlation function measured for the Center for Astrophysics (CfA) magnitude-limited redshift surveys.

2. THE PVDF FROM $n(\sigma)$

Suppose that the probability of measuring one component u of the relative velocity of two galaxies within a particular system is a universal function $\Lambda(u, \sigma)$, where σ is the velocity dispersion of the system and u is independent of the galaxy separation distance. Assume that $n(\sigma)$ is the number density of systems with dispersion σ. Moreover, assume that the number of galaxies ν within a system with dispersion σ depends only on σ: $\nu = \nu(\sigma)$. The probability of choosing a single galaxy is $n(\sigma)\nu(\sigma)$, and the probability of picking a galaxy pair within a single system is $n^2(\sigma)\nu^2(\sigma)/n(\sigma)$. Assume, for the sake of simplicity, that all the systems are disjoint with separation $\gtrsim 1\ h^{-1}$ Mpc. Thus, the contribution to the pairwise velocity distribution $p(u)$ for galaxy separation $\lesssim 1\ h^{-1}$ Mpc comes only from galaxy pairs in the same system. Therefore, we can neglect the relative velocities of systems. Then we have

$$p(u, \sigma_{\min}, \sigma_{\max})du \propto du \int_{\sigma_{\min}}^{\sigma_{\max}} \nu^2(\sigma) n(\sigma) \Lambda(u, \sigma) d\sigma \ . \quad (2.1)$$

Hereafter, we refer to equation (2.1) as the PVDF. Let us now make a few hypotheses that roughly approximate the internal properties of galaxy systems. Let us assume that systems have relaxed violently (Lynden-Bell 1967; Shu 1978). We can then assume that systems approximate truncated singular isothermal spheres with density profile $\rho(r) = \sigma^2/2\pi G r^2$. N-body simulations (Crone, Evrard, & Richstone 1994; Carlberg 1994; Navarro, Frenk, & White 1996; Cole & Lacey 1996) show that this profile is not correct at very small and very large radii. However, the slope r^{-2} fits the dark halo density profile at least over the range $0.1 \lesssim r/r_{\rm vir} \lesssim 1$, where $r_{\rm vir}$ is the radius containing an overdensity of 200 (Navarro et al. 1996).We are interested in the relation between the galaxy number ν and the velocity dispersion σ; thus, the assumption $\nu(\sigma) \propto \sigma^2$ is reasonable. The isothermal model has a Gaussian velocity distribution. Thus,

$$\Lambda(u, \sigma)du = \frac{1}{(4\sigma^2\pi)^{1/2}} \exp\left(-\frac{u^2}{4\sigma^2}\right)du \ . \quad (2.2)$$

We have two choices for the number density $n(\sigma)$: (1) we can assume the distribution derived from the Press & Schechter (1974) theory that approximates the number density of massive halos in N-body simulations of a flat universe with scale-free initial conditions (see, e.g., Efstathiou et al. 1988; Lacey & Cole 1994), or (2) we can use the observed distribution.

The Press-Schechter $n(\sigma)$ can be easily derived for a flat CDM universe dominated by dissipationless dark matter. Following White & Frenk (1991), consider spherical perturbations with comoving radius r_0 that have already collapsed into isothermal spheres by redshift z. For singular isothermal halos, the velocity dispersion is $\sigma^2 = GM(r)/2r$, independent of radius r. If the halo mass is $M = 4\pi\rho_0 r_0^3/3$, where ρ_0 is the present density of the universe, the velocity dispersion can be expressed in terms of the redshift and the initial size of the perturbation: $\sigma = 1.68(1 + z)^{1/2} H_0 r_0/2^{1/2}$, where H_0 is the present Hubble constant (however, see, e.g., Jing & Fang 1994 or Crone & Geller 1995 for mass-dispersion relations when the isothermal sphere approximation is not valid). The number of halos with dispersion σ per comoving volume at redshift z is then

$$n(\sigma)d\sigma = -\frac{3(1.68)^3 H_0^3 (1 + z)^{3/2}}{(4\pi)^{3/2}\sigma^4} \frac{d\ln\Delta}{d\ln\sigma} \nu e^{-\nu^2/2} d\sigma \ , \quad (2.3a)$$

where $\nu = \delta_c(1 + z)/\Delta$, and $\delta_c = 1.69$ is the mean linear interior mass overdensity when each spherical shell recollapses to the origin (Narayan & White 1988). The rms linear mass overdensity in a sphere of radius r_0 is

$$\Delta(r_0) = 16.3\, \sigma_8 (1 - 0.3909 r_0^{0.1} + 0.4814 r_0^{0.2})^{-10} \ , \quad (2.3b)$$

where σ_8^2 is the usual ratio of the variances of the mass and galaxy fluctuations within randomly placed spheres of radius $8\ h^{-1}$ Mpc. Equation (2.3b) approximates the correct $\Delta(r_0)$ to within 10% over the range $0.03\ h^{-1}$ Mpc $< r_0 < 20\ h^{-1}$ Mpc. The correct $\Delta(r_0)$ is obtained through the convolution of the CDM linear power spectrum with the spherical top-hat window function of radius r_0. The power spectrum, assuming $\Omega_0 = 1$, $h = 0.5$ and a cosmic microwave background temperature $\theta = 2.7$ K, is (Davis et al. 1985)

$$P(k) = 1.94 \times 10^4\, \sigma_8^2 \frac{k}{(1 + 6.8k + 72k^{3/2} + 16k^2)^2} \ {\rm Mpc}^3 \ . \quad (2.3c)$$

The only free parameter is now the nomalization parameter σ_8.

A sample of 25 Abell clusters with velocity dispersion $\sigma > 300$ km s^{-1} and 31 galaxy groups in the CfA redshift surveys with $\sigma > 100$ km s^{-1} (Zabludoff et al. 1993b) yields

$$n(\sigma)d\sigma \propto 10^{-\alpha\sigma} d\sigma \ , \quad (2.4)$$

where $\alpha = 0.0015$. Equation (2.4) holds for $\sigma > 700$ km s^{-1}. Mazure et al. (1996) analyze a volume-limited sample of 128 Abell clusters with richness $R \geq 1$. They find a similar $n(\sigma)$ with $\alpha \sim 0.0016$ for $\sigma > 800$ km s^{-1}. In both cases, the distribution is shallower for smaller σ. Thus, using equation (2.4) for the whole range of σ overestimates the number of system with small velocity dispersion. However, such an

overestimate does not affect our analysis. In fact, we shall see that we need even more systems with $\sigma < 700$ km s^{-1} to obtain an exponential PVDF.

With these assumptions, the integral in equation (2.1) at $z = 0$ yields the PVDFs in Figure 1 for different values of $\sigma_{\rm min}$ and for $\sigma_8 = 0.5$, 1.0, and 1.5, to map the range of *COBE* normalizations for different CDM models (Bunn, Scott, & White 1995). We set $\sigma_{\rm max} = 1500$ km s^{-1}.

If we decrease $\sigma_{\rm min}$, the Press-Schechter $n(\sigma)$ includes a larger fraction of halos of small size and peaks up the center of the distribution. However, most halos with $\sigma \lesssim 150$ km s^{-1} are likely to contain at most one galaxy as luminous as the Milky Way. Systems of galaxies with $\sigma \lesssim 100$ km s^{-1} are only a small fraction of the total number of systems predicted by the Press-Schechter theory at these velocity dispersions. Moreover, it is well known that the Press-Schechter $n(\sigma)$ for a flat CDM universe overestimates the observed number of single galaxy halos with $\sigma \lesssim 100$ km s^{-1} (see, e.g., White 1996). If we set $\sigma_{\rm min} \sim 100$ km s^{-1} as the lower limit of integration in equation (2.1), we mostly exclude halos containing only a single galaxy.

The observed $n(\sigma)$ does not include individual galaxies by definition and does not overestimate the number of galaxy systems with small σ. Therefore, the PVDF does not change appreciably for any choice of $\sigma_{\rm min}$.

Figure 1 shows that for reasonable values of $\sigma_{\rm min} \gtrsim 100$ km s^{-1}, equation (2.1) predicts a PVDF that is almost exponential at large relative velocities u. However, the PVDF bends over at smaller u. In order to obtain an exponential core, we need a different model for $\Lambda(u, \sigma)$.

3. $\Lambda(u, \sigma)$ OF UNRELAXED SYSTEMS

It is well known that steady state self-gravitating systems cannot have exactly Gaussian velocity distributions because escaping stars deplete the high-velocity tails (see, e.g., King 1965, 1966). In fact, the isothermal sphere is the only self-gravitating system with a Gaussian velocity distribution. However, its mass is infinite, and real steady state systems tend only asymptotically to the Gaussian distribution (see, e.g., Padmanabhan 1990).

We should not expect a Gaussian distribution in galaxy systems for another reason: many observed galaxy systems—from groups to clusters—are unlikely to be relaxed. Most galaxy groups are still collapsing (see, e.g., Diaferio et al. 1993; Doe et al. 1995), and many clusters contain substructures that indicate that they are far from equilibrium (see, e.g., West, Jones, & Foreman 1995; Colless & Dunn 1996). Therefore, a single Gaussian is not a good approximation to their velocity distribution. Velocity distributions will depend on the initial conditions and on the dynamical state of the system. In general, there will not be a universal $\Lambda(u, \sigma)$ for all galaxy systems.

These arguments apparently show that the assumptions about the shape and the uniqueness of the distribution $\Lambda(u)$ in § 2 are inadequate. However, we can investigate what shape $\Lambda(u)$ tends to assume in a hierarchical clustering scenario, where either systems are virialized or they are still forming through the aggregation of virialized subunits.

To model the evolution of a cluster by accretion of subunits, the excursion set formalism (see, e.g., Bower 1991;

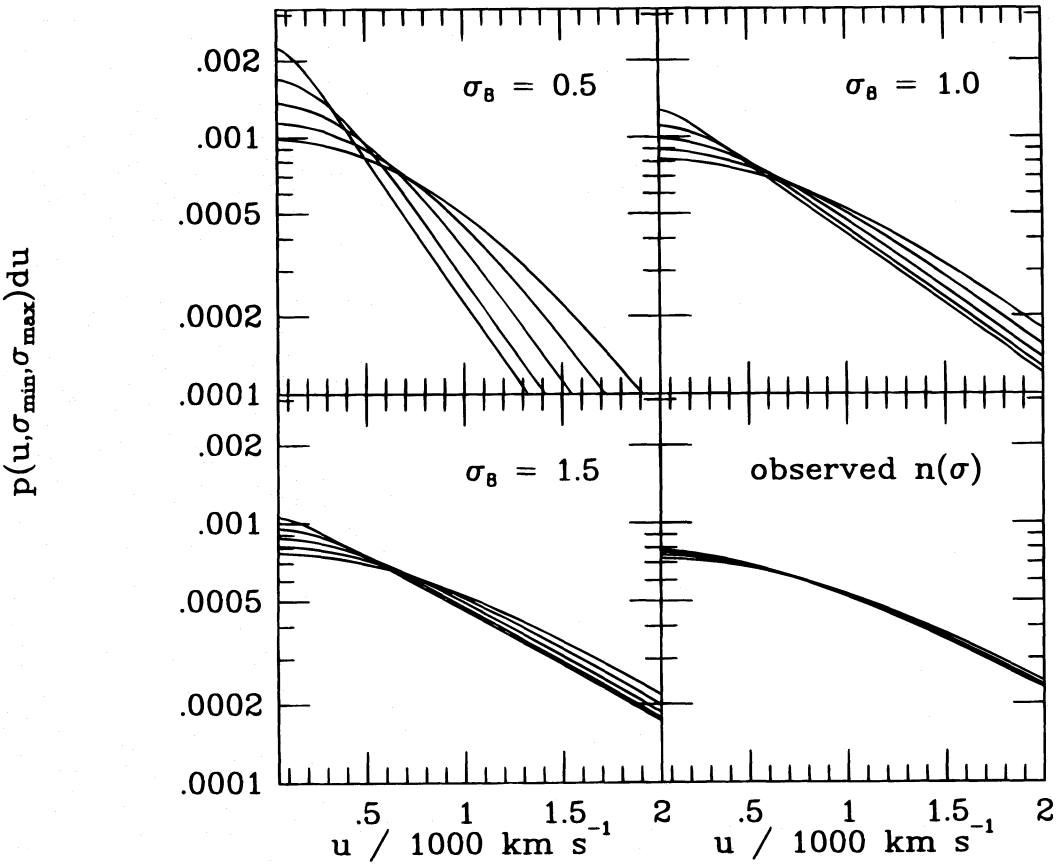

FIG. 1.—PVDF computed through eq. (2.1) with a Gaussian internal pairwise velocity distribution $\Lambda(u, \sigma)$. The number density of galaxy systems is the observed $n(\sigma)$ (eq. [2.4]) or the Press-Schechter $n(\sigma)$ for a flat CDM universe (eqs. [2.3]) with different normalization σ_8. We take $\sigma_{\rm max} = 1500$ km s^{-1}. At large relative velocities u, from top to bottom, the curves in each panel have $\sigma_{\rm min} = 500$, 400, 300, 200, and 100 km s^{-1}, respectively.

Bond et al. 1991; Kauffmann & White 1993; Lacey & Cole 1993) extends the Press-Schechter formalism to estimate the number density of halos with mass M_1 at redshift z_1 which will merge at different times to form a single halo of mass $M_2 > M_1$ at redshift $z_2 < z_1$. We have

$$n(M_1, z_1 \mid M_2, z_2)dM_1 = \left(\frac{2}{\pi}\right)^{1/2} \frac{\rho_0}{M_1} \left|\frac{d\ln \Delta_1}{dM_1}\right| \frac{(\delta_1 - \delta_2)\Delta_1^2}{(\Delta_1^2 - \Delta_2^2)^{3/2}} \times \exp\left[-\frac{(\delta_1 - \delta_2)^2}{2(\Delta_1^2 - \Delta_2^2)}\right] dM_1 , \quad (3.1a)$$

where ρ_0 is the present density of the universe, Δ_i^2 $(i = 1, 2)$ is the variance of the linear overdensity in a sphere containing the mass M_i, and $\delta_i = 1.69/D(z_i)$ is the extrapolated linear critical overdensity for which perturbations with overdensity $\delta > \delta_i$ have collapsed at redshift z_i. $D(z_i)$ is the perturbation growth factor.

Following the procedure used to obtain the number density of halos with velocity dispersion σ (eq. [2.3a]), we can use equation (3.1a) to express the number density of halos with velocity dispersion σ_1 at redshift z_1 that will form a halo with dispersion σ_2 at redshift $z_2 < z_1$. In a flat CDM universe, $D(z_i) = (1 + z_i)^{-1}$. Mass and dispersion of each halo are related by $M_i = 4\pi\rho_0(r_0^{(i)})^3/3$ and $\sigma_i = 1.68(1 + z_i)^{1/2}H_0 r_0^{(i)}/2^{1/2}$. Equation (3.1a) becomes

$$n(\sigma_1, z_1 \mid \sigma_2, z_2)d\sigma_1 = -\frac{3(1.68)^3 H_0^3 (1 + z_1)^{3/2}}{(4\pi)^{3/2}\sigma_1^4} \times \frac{d\ln \Delta_1}{d\ln \sigma_1} \frac{\Delta_1^2}{\Delta_1^2 - \Delta_2^2} \tilde{\nu} e^{-\tilde{\nu}^2/2} d\sigma_1 , \quad (3.1b)$$

where $\tilde{\nu} = 1.69(z_1 - z_2)/(\Delta_1^2 - \Delta_2^2)^{1/2}$, and we express Δ_i with the approximation of equation (2.3b).

Let us now suppose that we observe a galaxy system at redshift $z_1 = z$ that has not yet collapsed but that still contains different substructures that will merge to form a single halo with velocity dispersion $\sigma_2 = \sigma_{\max}$ at a later epoch, e.g., $z_2 = 0$. We want to compute the probability $\Lambda(u)$ of measuring a velocity difference u between two galaxies within this collapsing system at redshift z.

If we assume that each subunit has a velocity distribution $\psi(v, \sigma)$, the probability of choosing a galaxy with velocity v within the system is

$$\alpha(v, \sigma_{\min}, \sigma_{\max}, z)dv \propto dv \int_{\sigma_{\min}}^{\sigma_{\max}} n(\sigma, z \mid \sigma_{\max}, 0)\nu(\sigma)\psi(v, \sigma)d\sigma , \quad (3.2a)$$

where $n(\sigma, z \mid \sigma_{\max}, 0)$ is given by equation (3.1b) and $\nu(\sigma)$ is the number of galaxies within each substructure as in § 2. For the sake of simplicity, equation (3.2a) ignores the relative velocities of the subunits. The inclusion of this effect will probably broaden the velocity distribution α. Thus, equation (3.2a) is conservative with respect to our purpose of investigating the departure of α from a Gaussian. Here, however, we limit our analysis to the simplest case.

We notice that equation (3.2a) is a velocity distribution decomposition if we look at it the other way around. In other words, we "build" the velocity distribution instead of decomposing it. For example, van der Marel & Franx (1993) decompose line profiles of elliptical galaxies in orthogonal Gauss-Hermite functions to quantify departures from Gaussian line profiles. Zabludoff, Franx, & Geller (1993a) apply a discrete version of this technique to the velocity distributions of eight rich Abell clusters. Here, we point out that the hierarchical clustering scenario naturally predicts that $\alpha(v)$ is a sum of elementary distributions.

Equation (3.2a) quantifies the degree of subclustering in a galaxy system. Comparison of equation (3.2a) with velocity distributions of real clusters may provide constraints on the density of the universe (see, e.g., Evrard et al. 1993; Jing et al. 1995). Moreover, extensions of equation (3.2a) can determine the rate of growth of clusters as a function of redshift (Lacey & Cole 1993).

Now we can write the pairwise velocity distribution $\Lambda(u)$ as

$$\Lambda(u, \sigma_{\min}, \sigma_{\max}, z)du \propto du \int \alpha(v_1)\alpha(v_2)\delta(|v_1 - v_2| - u)dv_1 dv_2 = du \int \alpha(v_1)\alpha(v_1 + u)dv_1 . \quad (3.2b)$$

Let us assume that the subunits are virialized and that each approximates an isothermal sphere. Therefore, $\psi(v, \sigma)$ is Gaussian and $\nu(\sigma) \propto \sigma^2$ as in § 2. Integration of equation (3.2b) yields the curves in Figure 2 for different values of $\sigma_{\max}$, i.e., for different masses of the final dark halo, and for $\sigma_{\min} = 100$ km s^{-1}. Figure 2 shows that as we decrease the redshift z, i.e., as we come closer to the formation of the final system, $\Lambda(u)$ approaches a Gaussian, as expected. At high redshift, the system is far from equilibrium, and $\Lambda(u)$ is more centrally peaked.

Is the presence of substructure the only physical process responsible for more centrally peaked $\Lambda(u)$'s? Formally, the presence of substructures implies that $\Lambda(u)$ is a weighted integral of elementary distributions (eqs. [3.2]). This assumption is common to other fields: weighted integrals of Gaussian distributions are also invoked to explain the exponential shape of molecular cloud emission lines (see, e.g., Ida & Taguchi 1996; but see also Miesch & Scalo 1995) or the small-scale velocity gradient distribution in turbulent flows (Castaing, Gagne, & Hopfinger 1990; see also She 1991).

However, there is a very simple example in gravitational dynamics, where a centrally peaked $\Lambda(u)$ does not originate from a weighted integral. Consider a collapsed region subject to secondary infall (Gunn & Gott 1972): infalling galaxies have small relative velocities and peak up the center of the distribution, whereas galaxies in the viralized region populate the exponential tails.

An N-body toy model illustrates this issue. Consider an isolated mass sphere with initial radial density $\rho(r) = (M/4\pi R^3)(R/r)^2$, where R is the radius and M is the total mass of the sphere. If each shell is initially expanding according to the Hubble flow $\dot{r}(0) = H_0 r_0$, the maximum expansion radius is $r_{\max} = r_0 \exp(B)$ at time $t_{\max} = H_0^{-1}(\pi B)^{1/2} \exp(B)P(1/2, B)$, where $B = H_0^2 r_0^2 R/2GM$ and $P(\alpha, x)$ is the incomplete gamma function.

We choose this density profile for two reasons: (1) The difference between the time and the radius at maximum expansion of two different shells grows exponentially and distinguishes the infall and the virialized regions clearly for our illustrative purpose, and (2) the viralized region has the quasi-equilibrium density profile r^{-2}. Thus, at the same time, we mimimize the relaxation process and isolate the effect due to the infall region.

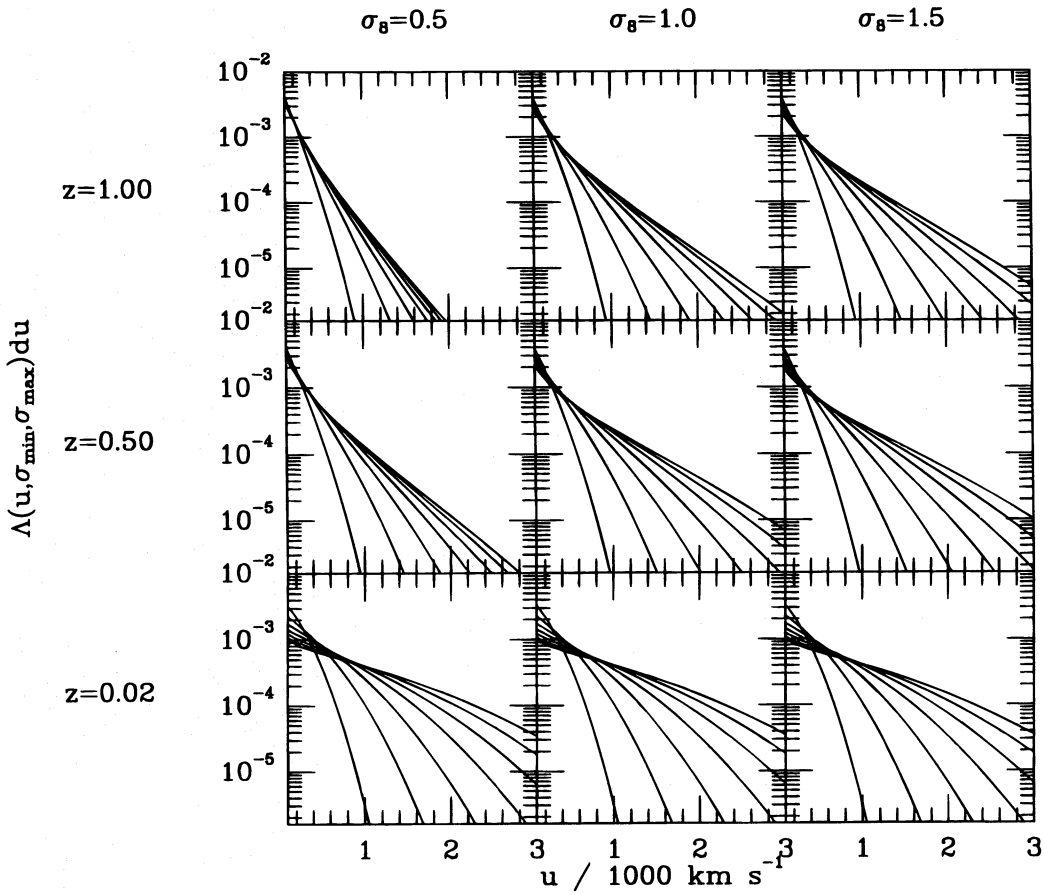

FIG. 2.—Pairwise velocity difference distribution $\Lambda(u)$ for a single unrelaxed galaxy system (eq. [3.2b]) at different redshift z and with different normalization σ_8. We take $\sigma_{min} = 100$ km s^{-1}. At large relative velocities u, from top to bottom, the curves in each panel have $\sigma_{max} = 1500$, 1300, 1100, 900, 700, 500, and 300 km s^{-1}, respectively.

We follow the evolution of an isolated spherical system with $N = 4096$ particles initially expanding with the Hubble flow. In numerical units, the gravitational constant is $G = 1$, the system has total mass $M = 1$ and radius $R = 1$, and the initial Hubble constant is $H_0 = 1.2$. We use the TREECODE by Hernquist (1987) with softening parameter $\epsilon = 0.02R$ and tolerance parameter $\theta = 0.8$. We integrate the particle equations of motion for two collapse times $t_c = 2\pi(3/10)^{3/2}GM^{5/2}/|E|^{3/2}$, where E is the total energy of the system. The integration time step is $\Delta t = 10^{-3}t_c$.

Figure 3*a* shows the evolution of the distribution of the velocity component v_z. We show three distributions at each time: the total distribution (*solid histogram*), the virialized region distribution (*bold histogram*), and the infall region distribution (*dashed histogram*). At each time t, particles with $4t_{max} \leq t$ belong to the virialized region, and particles with $4t_{max} > t$ belong to the infall region. We superimpose the best Gaussian fit on the virialized region distribution to show that virialization indeed took place in the central region. We choose the time limit $4t_{max} > 2t_{max}$ to suppress oscillation effects. Figure 3*a* clearly shows that the infall region is responsible for the central peak, and the virialized region is responsible for the tails of the total distribution. Figure 3*b* show that the total distribution in Figure 3*a* yield nearly exponential $\Lambda(u)$'s.

We also ran a simulation similar to the one above but with an initial density profile $\rho(r) = (M/2\pi R^3)(R/r)$ that yields $r_{max} = H_0^2 r_0^2/2B + r_0$ and $t_{max} = H_0 r_0/B$, where $B = GM/R^2$. The system relaxes faster than with an initial r^{-2} density profile, and secondary infall lasts for only a small fraction of the collapse time (Fig. 3*c*). However, when secondary infall involves a large mass fraction of the sphere, $\Lambda(u)$ is exponential (Fig. 3*d*).

Velocity distributions like those in Figure 3*a* are difficult to observe in individual real systems. Infall regions in which galaxies have small velocities relative to the center of mass of the cluster are close to the turnaround radius, which is $\gtrsim 1\ h^{-1}$ Mpc for a typical Abell cluster with mass $\sim 10^{14}\ h^{-1}\ M_\odot$, i.e., richness $R = 1$. Those regions are contaminated by foreground and background objects, and they are generally poorly sampled. Therefore, when systems are observed individually, observational biases imply that departures from Gaussian velocity distributions in observed clusters are more likely due to subclustering rather than to infall region effects. However, both effects are present in redshift surveys in which large regions of the universe are sampled.

The preceding discussion shows that unrelaxed systems imply that $\Lambda(u)$'s differ from Gaussians. The $\Lambda(u)$'s for unrelaxed systems tend to have a more pronounced central peak than Gaussian distributions. A combination of substructures and infall regions contribute to this shape.

It is now clear that a unique and universal $\Lambda(u, \sigma)$ does not exist, but rather each system has a distribution depending on its particular dynamical state. However, for the sake of investigation, we persist in the assumption of a universal

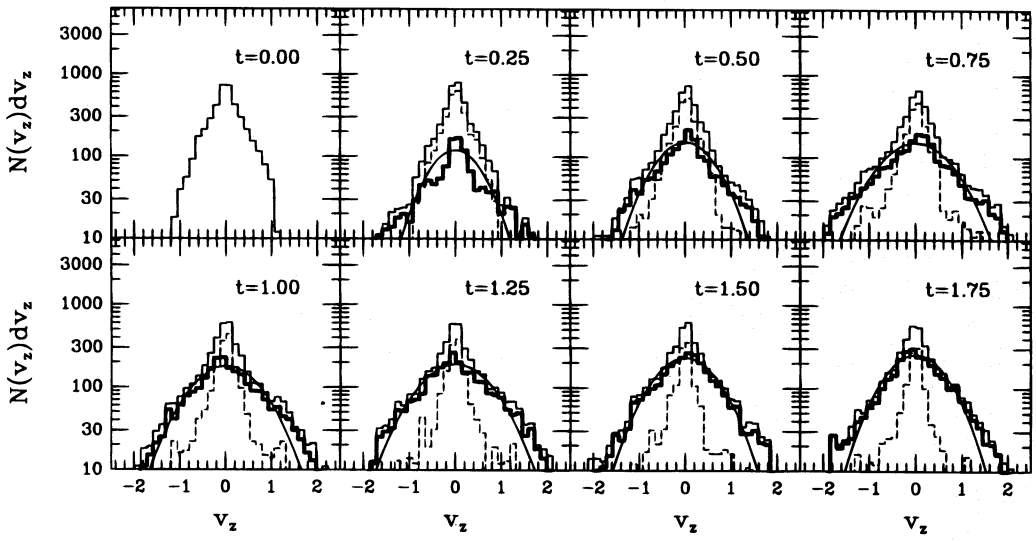

FIG. 3*a*

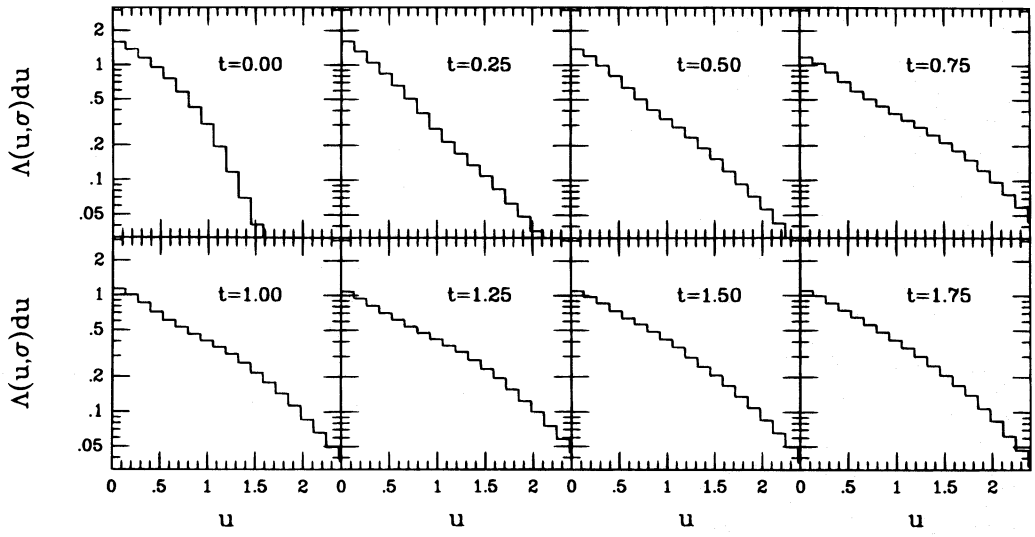

FIG. 3*b*

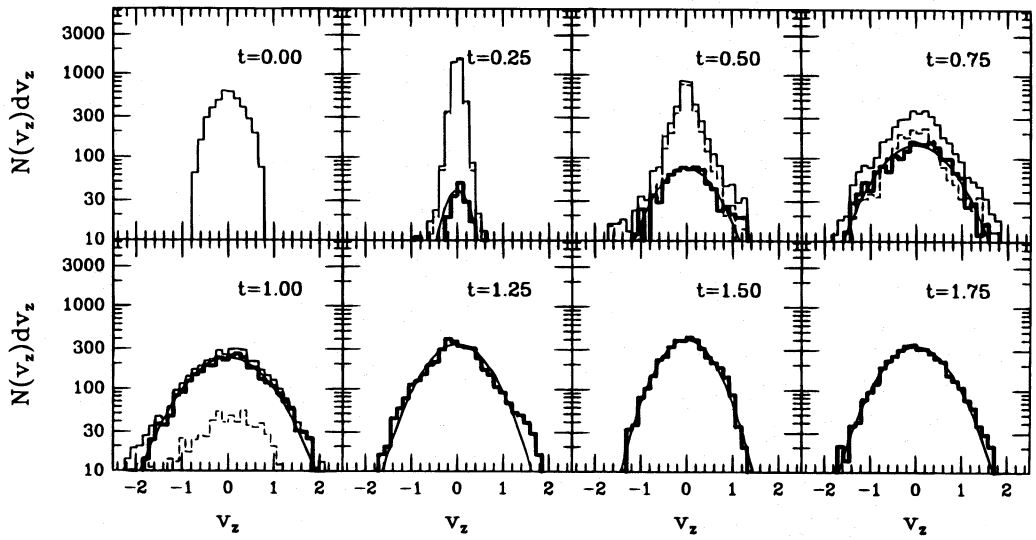

FIG. 3*c*

FIG. 3.—Evolution of the distribution of the velocity components v_z for an isolated spherical system of particles initially expanding with the Hubble flow and with (*a*) an initial r^{-2} density profile or (*c*) an initial r^{-1} density profile. Times are in units of the collapse time t_c. The solid histogram is the total distribution, the bold histogram is the distribution for particles within the virialized core, and the dashed histogram is for particles within the infall region. The curves are the best Gaussian fits to the viralized core distributions. Panels (*b*) and (*d*) show the evolution of the pairwise velocity difference distribution $\Lambda(u)$ for the system with initial r^{-2} or r^{-1} density profiles, respectively.

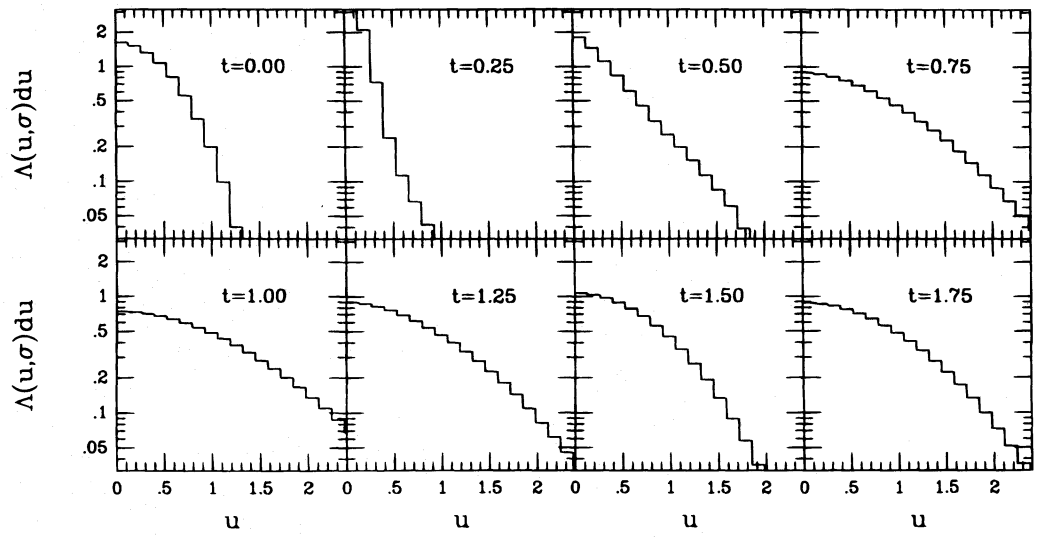

FIG. 3*d*

$\Lambda(u)$, and we examine the way the PVDF $p(u)$ in equation (2.1) changes when $A(u, \sigma)$ differs from a Gaussian, Figures 2 and 3 suggest that systems far from equilibrium may have a distribution similar to an exponential:

$$\Lambda(u, \sigma)du = \frac{1}{\sigma\sqrt{2}} \exp\left(\frac{-\sqrt{2}|u|}{\sigma}\right)du . \qquad (3.3)$$

With an exponential $\Lambda(u)$, the integral in equation (2.1) yields the curves in Figure 4. We clearly see that the central peak is more pronounced than in the Gaussian case (Fig. 1) yielding a better approximation to an "exponential" shape for the PVDF.

We stress here that the results of Figures 1 and 4 are based on the generic assumption that all galaxy systems have the same internal pairwise velocity distribution $\Lambda(u, \sigma)$. However, the use of a unique $\Lambda(u, \sigma)$ is still meaningful if we interpret $\Lambda(u, \sigma)$ as a convolution of different internal pairwise velocity distributions of individual systems at different dynamical states but with the same σ. Thus, the results of

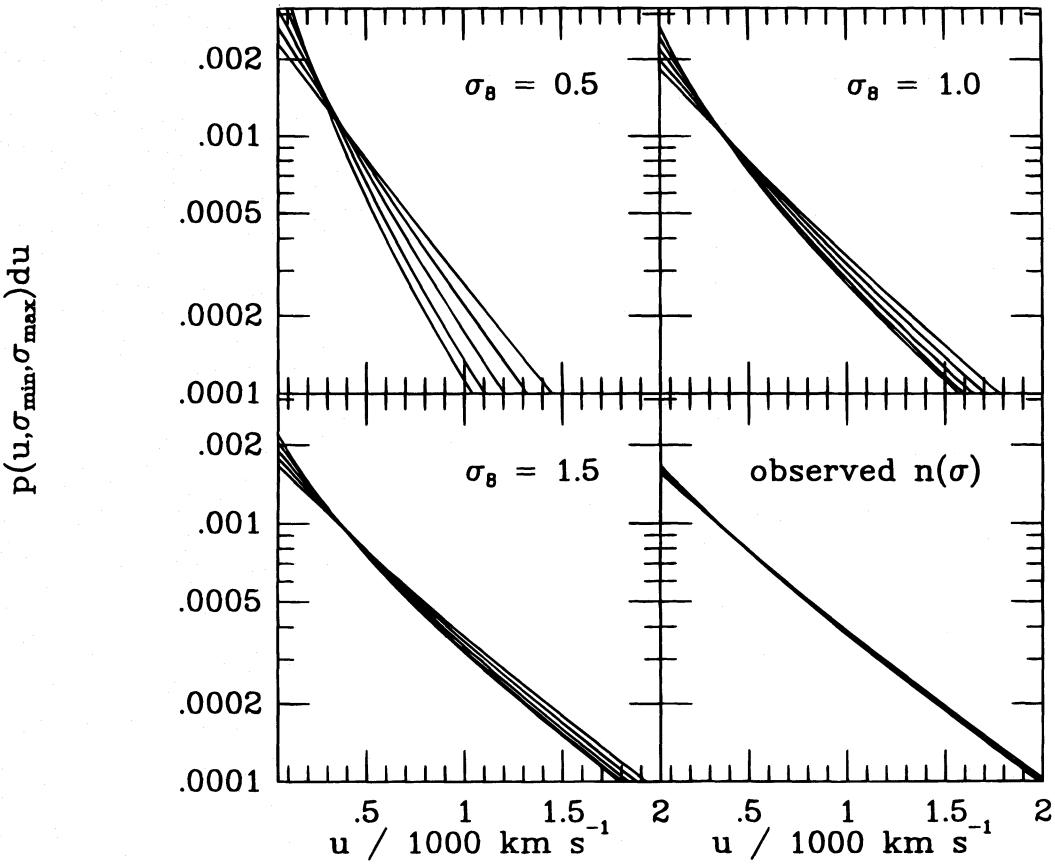

FIG. 4.—Same as Fig. 1, but with an exponential $\Lambda(u, \sigma)$ (eq. [3.3])

Figures 1 and 4 allow us to conclude that if the real PVDF is indeed exponential over a wide range of relative velocities u, the blend of different internal pairwise velocity distributions must contain a large fraction of distributions more centrally peaked than a Gaussian. In other words, the exponential shape of the PVDF is a signature of the presence of a large fraction of unrelaxed systems.

4. $\Lambda(u, \sigma)$ OF DISSIPATIVE SYSTEMS

In § 3 we show that unrelaxed systems have internal pairwise velocity distribution $\Lambda(u, \sigma)$ more centrally peaked than a Gaussian. This shape arises from secondary infall and the presence of substructures. Here, we investigate a third physical process that can peak up the $\Lambda(u)$ distribution at small relative velocities: the transfer of orbital kinetic energy to galaxy internal degrees of freedom. In fact, this effect has only a secondary impact on the velocity distribution.

To examine this issue, one should solve the complete Boltzmann equation for the evolution of the phase space density of the galaxy system including a collisional term. Fusco-Femiano & Menci (1995) study how the velocity distribution evolves in the presence of binary mergers in an external gravitational potential. In other words, they compute the decrease of orbital kinetic energy when binaries disappear by merging. Here, we want to include the orbital kinetic energy loss due to tidal perturbations, thus computing the energy loss when mergings do not take place.

We assume a simple physical model to derive an analytic expression for the expected $\Lambda(u)$. Assume an initially stable self-gravitating gas of particles. Imagine switching on the particle internal degrees of freedom at a time t_0. Now, during the motion of particles within the system, tidal effects increase the particle internal energy at the expense of the orbital kinetic energy of the particles. This system is apparently unstable, tending ultimately to a general merging of "hot" particles. This process indeed occurs in galaxy groups (see, e.g., Mamon 1992b; Diaferio et al. 1993; Doe et al. 1995; Weil & Hernquist 1996).

The most serious shortcoming of this model is that we assume a constant particle mass, clearly incorrect because merging and tidal stripping are ongoing processes. Both processes increase the kinetic energy loss. When galaxies merge, a binary system disappears, and its relative kinetic energy is completely transferred to the internal energy of the remnant. Tidally stripped matter forms a common background envelope. Particle cores also lose kinetic energy through dynamical friction against this background. Therefore, the main consequence of ignoring mass loss is to underestimate the kinetic energy loss.

However, with these hypotheses and the assumption that the unperturbed velocity distribution is Gaussian, we derive the perturbed distribution (see the Appendix)

$$\Lambda(u, \sigma)du = \tilde{C}(\sigma, \alpha, \varphi) \exp\left(-\frac{u^2}{4\sigma^2}\right) \times \left[1 - \alpha\tilde{H}\left(\frac{u}{\sigma\sqrt{2}}, \varphi\right)\right]du , \quad (4.1a)$$

where $\tilde{C}$ is the normalization constant, and the function $\tilde{H}$ can be expressed in terms of the modified Bessel functions. In addition to the velocity dispersion σ, this distribution depends on two parameters α and φ. If we identify particles with galaxies, both α and φ contain information about the similarity of the galaxy internal dynamics to the galaxy system dynamics. In fact,

$$\varphi \propto \frac{\sigma_i}{\sigma}\frac{p_{\min}}{r_c} \quad (4.1b)$$

and

$$\alpha \propto \left(\frac{\sigma_i}{\sigma}\right)^4 \frac{r_c}{R_s} , \quad (4.1c)$$

where σ_i is the velocity dispersion of the stars within an individual galaxy; r_c and R_s are the galaxy and the system size, respectively; and $p_{\min}$ is the maximum separation at which two interacting galaxies are considered a merger remnant.

In order to test the hypotheses leading to equations (4.1), we follow the evolution of a King sphere (King 1966) with Hernquist's (1987) N-body code. King spheres have a truncated Gaussian velocity distribution and are stable self-gravitating systems. Therefore, they approximate the boundary conditions of our physical model.

We sample two King spheres with central gravitational potential $\phi(0)/\sigma^2 = -12$. The system sphere contains $N_g = 50$ particles; the galaxy sphere contains $N_s = 100$ particles. We evolve each sphere in isolation for 4.8 collapse times t_c. We set the tolerance parameter $\theta = 0.8$ and the time step $\Delta t = 10^{-3}t_c$. A softening parameter $\epsilon = 0.1r_t$, where r_t is the tidal radius of the sphere, ensures suppression of two-body relaxation effects. As expected, the spheres are dynamically stable, and their velocity distributions remain remarkably Gaussian for the entire integration.

We then replace each particle of the final system sphere with a 100 particle final galaxy sphere. In other words, the 50 single particles become resolved "galaxies" containing 100 particles each. We opportunely rescale particle velocities and relative positions to ensure dynamical equilibrium and to suppress two-body relaxation within each galaxy. This procedure is equivalent to switching on the particle internal degrees of freedom. We evolve the system for $2.4t_c$. Simulation units are $G = M = R = 1$, where G is the gravitational constant, M is the total mass, and R is the radius of the system. At each time, we identify galaxies from particle positions through a generalization of the friends-of-friends algorithm (Diaferio, Geller, & Ramella 1994). After $2.4t_c$ the galaxy number usually decreases from 50 to ~ 30.

We ran five simulations with different random number seeds. Figure 5 shows the time evolution of the distribution $\lambda(u)$ of the galaxy pairwise velocity difference moduli. Differences among the distributions of the five simulations arise from statistical effects only. Thus, in Figure 5 we suppress statistical noise by summing the distributions of the five simulations at each time. Two fits are superimposed: the bold curve is the perturbed Maxwellian distribution given in the Appendix (eqs. [A12])

$$\lambda(u)du = C(\sigma, \alpha, \varphi)u^2 \exp\left(-\frac{u^2}{4\sigma^2}\right) \times \left[1 - \alpha H\left(\frac{u}{\sigma\sqrt{2}}, \varphi\right)\right]du , \quad (4.2)$$

and the solid curve is the Maxwellian distribution, i.e., equation (4.2) when $\alpha = 0$.

In the perturbed Maxwellian, we set $\varphi = 1.22$ according to equation (A4); σ and α are free parameters. By adding φ

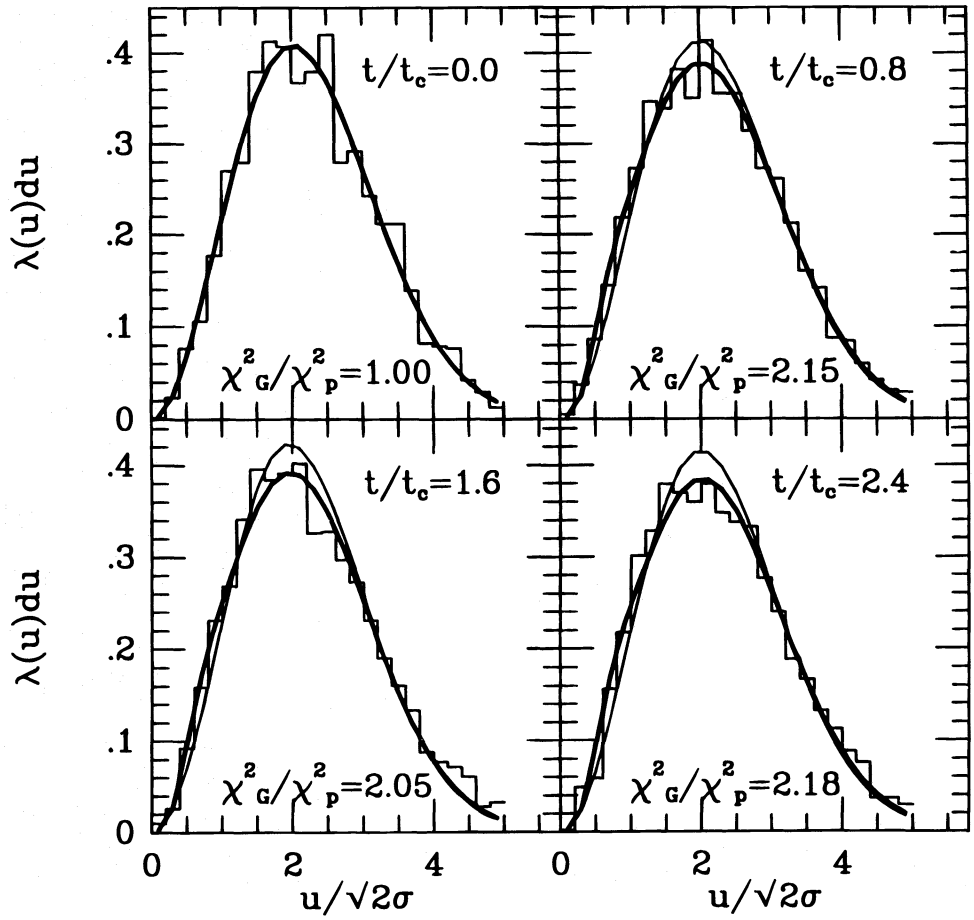

FIG. 5.—Time evolution of the distribution of pairwise velocity difference moduli for systems of particles with internal degrees of freedom. The distribution is initially Maxwellian, but at later times the frequency of small relative velocities increases. The best Maxwellian fits (*solid lines*) and the eq. (4.2) fits (*bold lines*) are shown. The latter are slightly better than the former as shown by the ratios of the χ^2's. In simulation units, the Maxwellians have fit parameters $2^{1/2}\sigma = 1.43$, 1.42, 1.39, and 1.41 at $t/t_c = 0.0$, 0.8, 1.6, and 2.4, respectively. The perturbed Maxwellians have fit parameters $2^{1/2}\sigma = 1.44$, 1.45, 1.41, and 1.44 and $\alpha = 0.01$, 0.13, 0.14, and 0.15, respectively.

as a free parameter, the fits do not change significantly, and φ remains in the range 1.00–1.40. Therefore, the perturbed Maxwellian only has α as an additional free parameter compared with the Maxwellian distribution. Figure 5 shows that the perturbed Maxwellian describes the increased frequency of small relative velocities. However, the frequency increase is barely detectable, despite the fact that typically $\sigma_i/\sigma \sim 0.9$ (eq. [4.1c]); i.e., the ratio of the velocity dispersions is not negligible. The ratio of the χ^2's of the two distributions shows that the perturbed Maxwellian fits the numerical distribution only slightly better than the Maxwellian distribution.

At earlier times ($t \lesssim 2t_c$), most galaxies have not yet merged, and their masses have not been reduced significantly by tidal stripping. Therefore, the physical model outlined in the Appendix is approximately valid. When we follow the system evolution for $t > 2.4t_c$, we find that $\lambda(u)$ does not usually tend to depart farther from the unperturbed distribution. At these later times, however, comparison of equation (4.2) with the numerical distributions is meaningless. Mergers create one large merger remnant surrounded by galaxies with masses $\lesssim 0.1$ times the dominant galaxy mass. Thus, the system no longer contains galaxies similar in mass, and our simple physical assumptions break down.

Thus, Figure 5 confirms that $\Lambda(u, \sigma)$ in equation (4.1a) should be valid for galaxy systems containing galaxies of similar mass. However, if $\Lambda(u, \sigma)$ is Gaussian in the absence of galaxy internal degrees of freedom, we expect that small departures from a Gaussian distribution will arise from the transfer of energy to the internal degrees of freedom.

In order to test equation (4.1a) against $\Lambda(u)$'s of real systems, we compare equation (4.1a) with Hickson's compact groups (Hickson 1993). These systems are the densest in the universe ($\sim 10^5$ galaxies per h^3 Mpc^{-3}) if they are not two-dimensional projections of unrelated galaxies (Mamon 1992a; Hernquist, Katz, & Weinberg 1995). Therefore, we expect that the kinetic energy loss effects might be detectable in these extreme systems. Moreover, Hickson's brightness selection criterion requires that galaxy members lie within an interval of 3 mag, assuring that galaxy members are not very different in mass.

Figure 6 shows $\Lambda(u)$ for the 69 Hickson (1993) compact groups with $N \geq 4$ galaxies. We sum all the single distributions for the whole sample of 69 compact groups because we assume that each compact group is a sample of the same parent distribution. We base this approach on the model first proposed by Diaferio, Geller, & Ramella (1994, 1995) that observed compact groups may be identified with substructures in collapsing rich loose groups. Ramella et al.

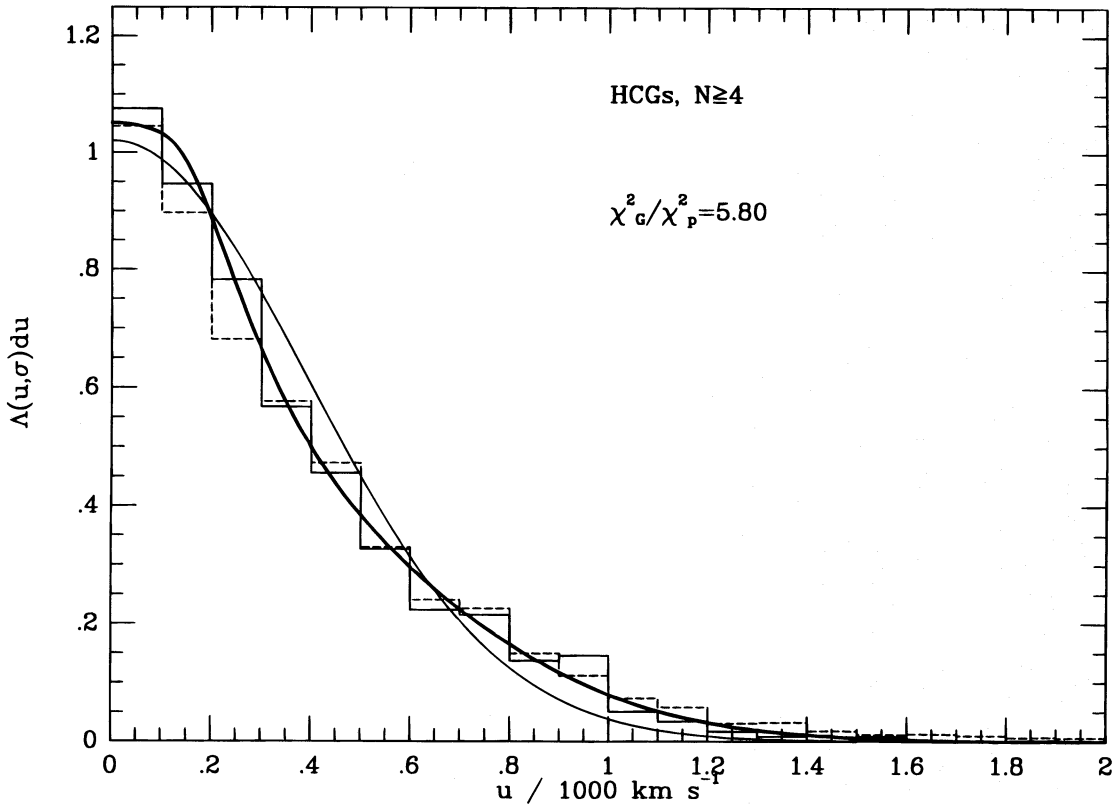

FIG. 6.—Galaxy pairwise velocity difference distribution for the 69 Hickson compact groups with $N \geq 4$ members. The solid line is the best-fit Gaussian, and the bold line is the best-fit perturbed Gaussian (eq. [4.1a]). The Gaussian has fit parameter $2^{1/2}\sigma = 391$ km s^{-1}. Eq. (4.1a) has fit parameters $2^{1/2}\sigma = 487$ km s^{-1} and $\alpha = 0.69$. The dashed histogram is the pairwise velocity difference distribution for the compact groups with $N \geq 4$ members in the simulated catalog of Diaferio et al. (1995).

(1994) search the redshift neighborhoods of compact groups within the CfA magnitude-limited redshift surveys and confirm that at least 70% of compact groups are embedded in larger systems. If compact groups share this same origin, we may assume that the pairwise velocity distribution of each compact group is sampled from the same parent distribution.

Equation (4.1a) (*bold curve*) clearly fits the observed distribution better than a Gaussian distribution (*solid curve*). This result indicates that compact group galaxies are loosing kinetic energy in a way consistent with our simple physical model. Moreover, $\Lambda(u, \sigma)$ is only slightly perturbed compared with a Gaussian, which indicates that the galaxies still retain most of their orbital kinetic energy. This conclusion agrees with the hypothesis that compact groups have just collapsed and that most galaxies are at their first encounter within the compact group (Diaferio et al. 1994).

Figure 6 shows a further confirmation of the validity of this model of the formation of compact groups. The dashed histogram is the pairwise velocity distribution computed from the simulated catalog of compact groups with $N \geq 4$ members (Diaferio et al. 1995). The Kolomogorov-Smirnov test shows that the observed compact group sample and the simulated sample belong to the same parent distribution at the 16% significance level.

However, the difference between the two distributions is not a statistical effect: the N-body model systematically underestimates the frequency of small relative velocities. This result suggests that the model dynamical resolution is insufficient to resolve the transfer of kinetic energy completely. In other words, the model tends to merge galaxies before Nature does. This result is expected: the model only accounts for dissipationless galaxy formation processes. Dissipative processes decrease the galaxy merging cross sections, and the galaxies survive for a longer time against merging than in dissipationless N-body simulations (see, e.g., Evrard, Summers, & Davis 1994; Frenk et al. 1996).

We finally consider the pairwise velocity distribution for a galaxy cluster. The perturbed distribution in equation (4.1a) depends on the fourth power of the ratio between the internal velocity dispersion of individual galaxies and the velocity dispersion of the galaxies within the cluster (eq. [4.1c]). Thus, we expect a nearly Gaussian $\Lambda(u, \sigma)$ for a massive virialized cluster. We consider the Abell cluster A576 (Mohr et al. 1996). The 85% complete magnitude-limited sample contains 169 galaxies lying within a projected distance $r \lesssim 1.5\ h^{-1}$ Mpc. The cluster mass lies in the range ~ 1–$4 \times 10^{15}\ h^{-1}\ M_\odot$, which implies a turnaround radius $\sim 3.0\ h^{-1}$ Mpc. Therefore, the infall region around the turnaround radius is not sampled. Of the 169 galaxies within the central region, 58 galaxies have spectra with line emission, and 111 have no line emission. Mohr et al. (1996) identify these two samples with galaxies containing or not containing star formation regions, respectively. They also generically identify them with late-type or early-type galaxies. Mohr et al. (1996) show that the late-type galaxies have a velocity distribution broader than the early-type galaxies and identify late-type galaxies with galaxies falling into the central region for the first time. Thus, if we exclude these galaxies, the subsystem of early-type galaxies is in approximate virial equilibrium. Mohr et al. (1996) argue that the absence of apparent substructures in the distribu-

tion of the early-type galaxies confirms this assumption. Figure 7 shows the pairwise velocity distribution for the non–emission-line galaxies only. In contrast with the compact group sample in which $\sigma_i/\sigma \sim 1$, here we have $\sigma_i/\sigma \sim 0.3$ (eq. [4.1c]). We fit the distribution with σ and α free parameters; $\varphi = 1.22$ as for the numerical experiment. As expected from equation (4.1c), the Gaussian and equation (4.1a) fit the observed distribution equally well.

5. THE REDSHIFT-SPACE CORRELATION FUNCTION

In the preceding sections we investigate how the exponential shape of the PVDF depends on the galaxy system number density $n(\sigma)$ and the internal galaxy pairwise velocity distribution $\Lambda(u, \sigma)$ of individual systems. We assume that all the galaxy systems have the same $\Lambda(u, \sigma)$. We then investigate how $\Lambda(u, \sigma)$ varies depending on the internal dynamics of each system.

We now investigate how the redshift space correlation function ξ_s depends on the galaxy system number density $n(\sigma)$ and $\Lambda(u, \sigma)$ through the PVDF. We restrict ourselves to Gaussian and exponential $\Lambda(u, \sigma)$'s. We do not discuss the $\Lambda(u)$ distribution for dissipative systems (§ 5), because this distribution is only marginally distinguishable from a Gaussian for real systems.

The "convolution method" (see, e.g., Fisher 1995) expresses the redshift-space correlation function ξ_s as

$$1 + \xi_s(r_p, \pi) = \int_{-\infty}^{+\infty} [1 + \xi(r)]p(u)dy \,, \qquad (5.1)$$

where r_p is the spatial separation of the galaxy pair projected on the sky, π is the velocity difference along the line of sight, $r^2 = r_p^2 + y^2$, y is the pair spatial separation parallel to the line of sight, and $u = \pi - y$ is the peculiar relative velocity;[2] $\xi(r)$ is the real-space correlation function, and $p(u)$ is the PVDF. In equation (5.1) we assume (1) that the PVDF is independent of r and (2) that the mean relative peculiar velocity $v_{12}(r)$ of galaxy pairs separated by r is zero. Both assumptions are reasonable when $0.1\ h^{-1}$ Mpc $\lesssim r_p \lesssim 1\ h^{-1}$ Mpc, where galaxy velocities are almost random [$v_{12}(r) \sim 0$] and the pairwise velocity dispersion $\sigma_{12}(r) \sim$ const (Marzke et al. 1995; Fisher 1995).

We consider the redshift-space correlation function averaged over the projected separation r_p, namely,

$$\langle \xi_s(r_{\min}, r_{\max}, \pi) \rangle = \frac{1}{r_{\max} - r_{\min}} \int_{r_{\min}}^{r_{\max}} \xi_s(r_p, \pi) dr_p \,. \qquad (5.2)$$

Figure 8 shows the comparison of the measured $\langle \xi_s(\pi) \rangle$ for different intervals of projected separations $[r_{\min}, r_{\max}]$ with different models of the PVDF convolved with the real-space correlation function $\xi(r)$. We use $\xi(r) = (r/r_0)^{\gamma}$, where $r_0 = 5.97 \pm 0.15\ h^{-1}$ Mpc and $\gamma = -1.81 \pm 0.02$ as measured by Marzke et al. (1995) for the CfA redshift survey (CfA2) and the Southern Sky Redshift Survey (SSRS2) galaxy samples combined (CfA2 + SSRS2). In Figure 8, squares are the measured $\langle \xi_s(\pi) \rangle$ for this sample with $[r_{\min}, r_{\max}] = [0.1, 0.2]$, [0.2, 0.4], [0.4, 0.8], and [0.1, 1.0] h^{-1} Mpc. We superimpose the curves computed through the integrals in equations (5.2) and (5.1), where $p(u)$ is the inte-

[2] Here we assume that the velocities are in units of the present Hubble constant H_0.

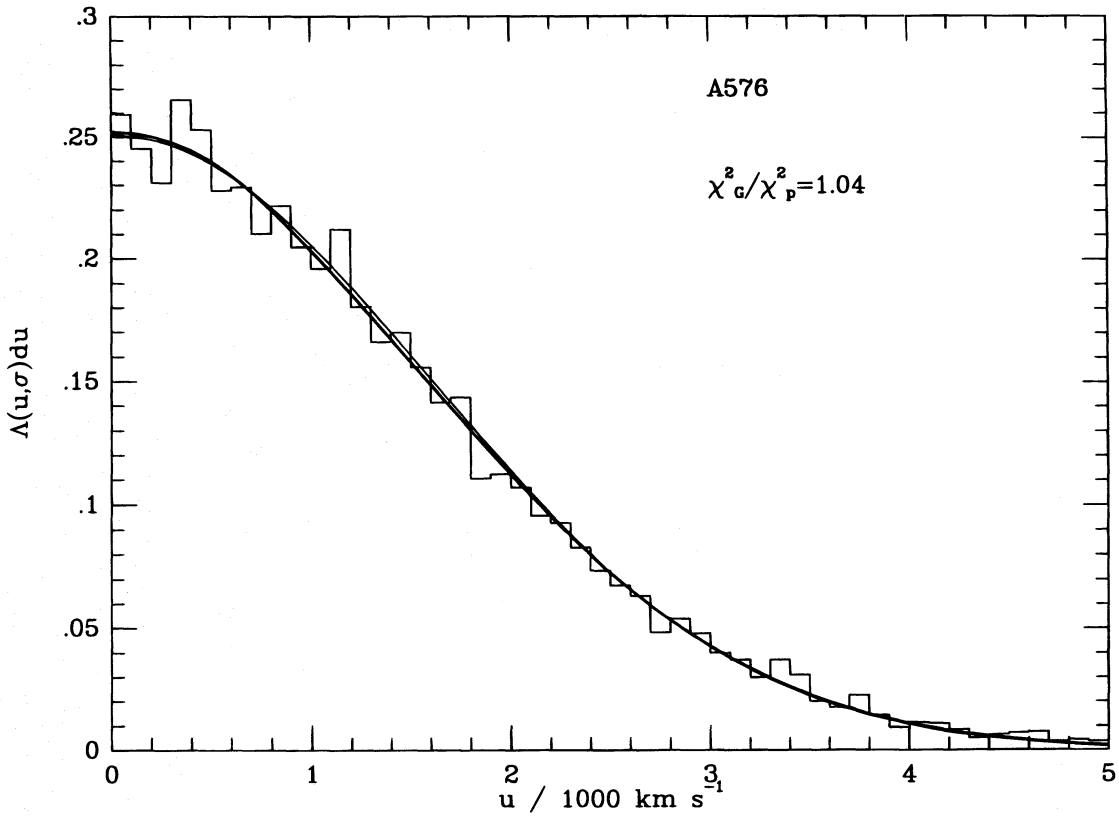

FIG. 7.—Galaxy pairwise velocity difference distribution for the central region of the Abell cluster A576. The solid line is the best-fit Gaussian, and the bold line is the best-fit perturbed Gaussian (eq. [4.1a]). The ratio of the χ^2's shows that the two fits do not differ. The Gaussian has fit parameter $2^{1/2}\sigma = 1589$ km s^{-1}. Eq. (4.1a) has fit parameters $2^{1/2}\sigma = 1607$ km s^{-1} and $\alpha = 0.05$.

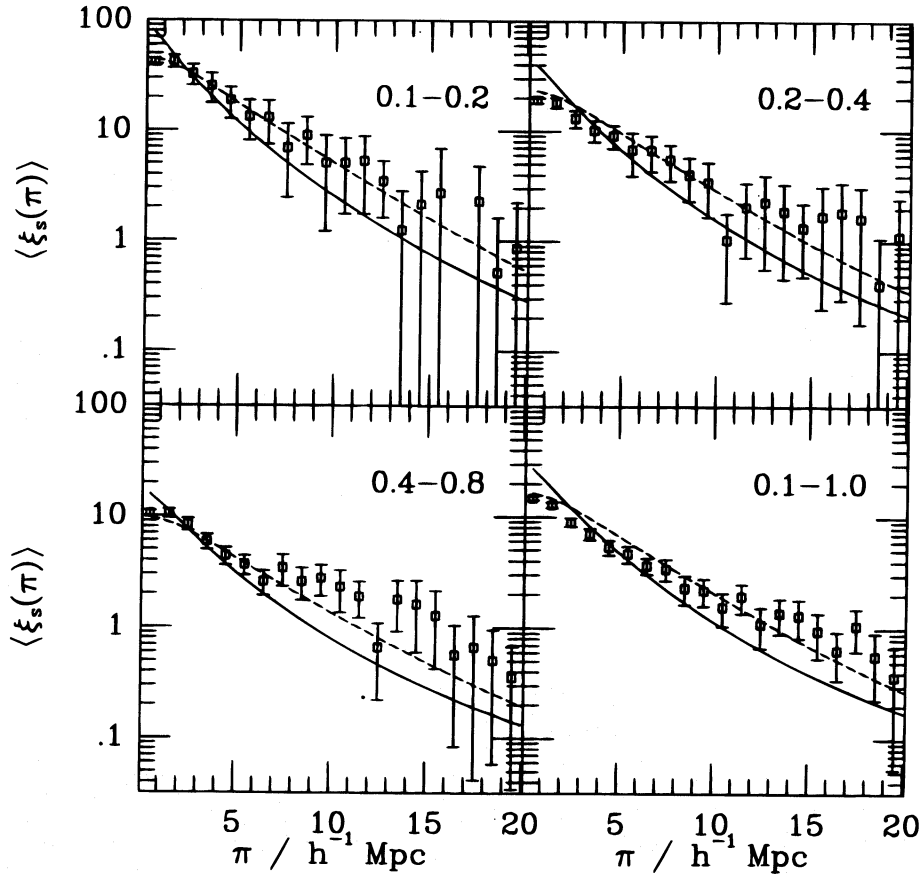

FIG. 8a

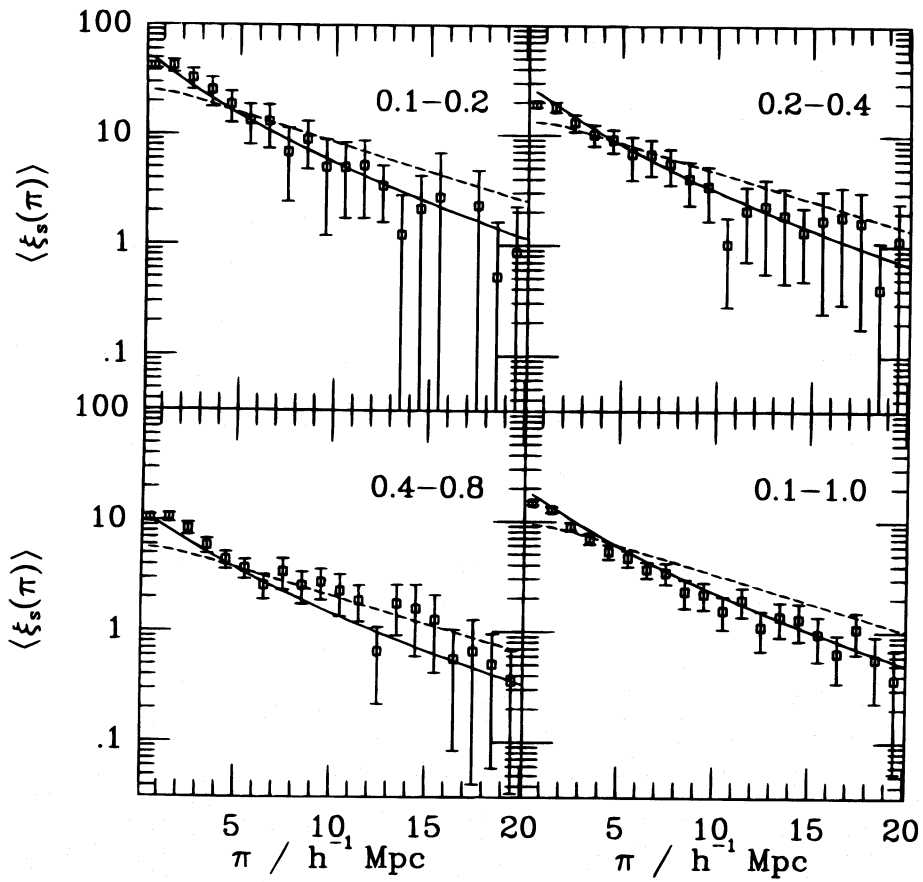

FIG. 8b

FIG. 8.—Comparison of the observed redshift-space correlation function $\langle \xi_s(\pi) \rangle$ with models of the PVDF convolved with the observed real space correlation function (eqs. [5.2] and [5.1]). Squares are the measures from the CfA2 + SSRS2 redshift survey samples with $[r_{min}, r_{max}] = [0.1, 0.2]$, $[0.2, 0.4]$, $[0.4, 0.8]$, and $[0.1, 1.0]h^{-1}$ Mpc, respectively, as shown in each panel (Marzke et al. 1995). Curves are the PVDFs (eq. [2.1]) with $\sigma_{min} = 100$ km s^{-1} and $\sigma_{max} = 1500$ km s^{-1}. Solid (dashed) lines are computed with an exponential (Gaussian) internal pairwise velocity distribution $\Lambda(u, \sigma)$. The number density of galaxy system is the observed $n(\sigma)$ (eq. [2.4]) or the Press-Schechter $n(\sigma)$ for a flat CDM universe (eq. [2.3a]) with different normalization σ_8: (*a*) $\sigma_8 = 0.5$; (*b*) $\sigma_8 = 1.0$; (*c*) $\sigma_8 = 1.5$; (*d*) observed $n(\sigma)$.

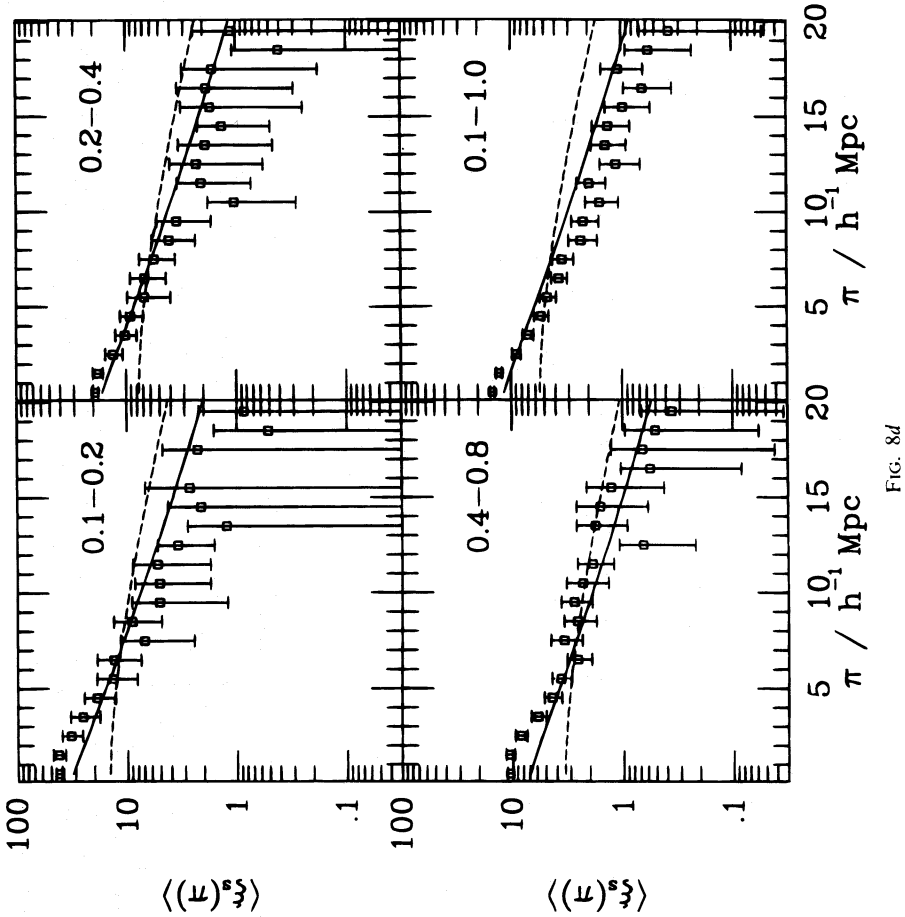

FIG. 8*d*

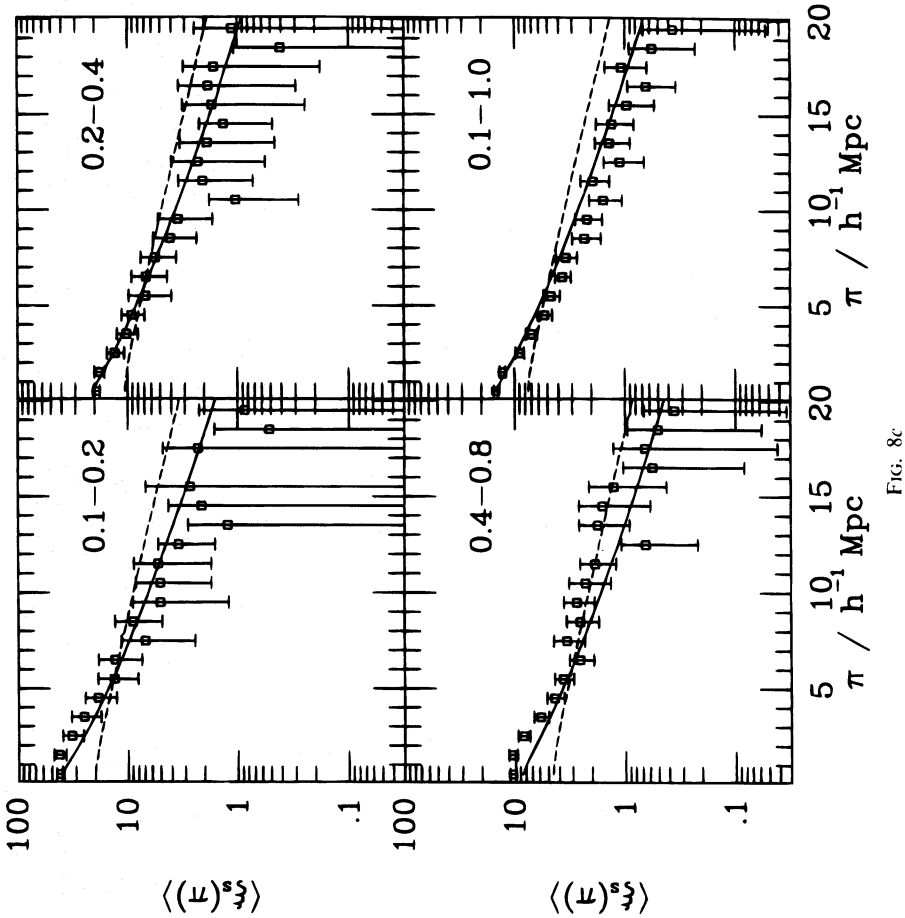

FIG. 8*c*

gral in equation (2.1) with $\sigma_{min} = 100$ km s^{-1} and $\sigma_{max} = 1500$ km s^{-1}. We show the curves with a Gaussian internal velocity distribution $\Lambda(u, \sigma)$ (*dashed lines*) and with an exponential $\Lambda(u, \sigma)$ (*solid lines*). We compute the curves with both the observed $n(\sigma)$ (eq. [2.4]) and with the distribution derived from the Press-Schechter theory (eq. [2.3a]) for $\sigma_8 = 0.5$, 1.0, and 1.5.

In order to quantify the agreement between the curves and the data for each projected separation interval, we plot the χ^2 per degrees of freedom ν as a function of the upper limit r_{max} of the interval (Fig. 9). We do not derive a parameter from the 20 data points within each range of r_p; thus, we assume $\nu = 20$. The χ^2's are indicative and are meaningful only if we compare them with each other. The data are actually correlated, and the estimates of $\langle \xi_s(\pi) \rangle$ are not normally distributed. Therefore, we should use a different approach to estimate χ^2 (see Fisher et al. 1994a and Marzke et al. 1995 for further details).

The observed $n(\sigma)$ approximates the data better when it weights an exponential $\Lambda(u)$ (Fig. 9 [*open squares*]) rather than a Gaussian (*filled squares*). However, systems selected from a redshift survey exceed a particular density contrast threshold $\delta\rho/\rho$. The $n(\sigma)$ we use thus contains only systems with $\delta\rho/\rho \geq 80$ with respect to the background (Zabludoff et al. 1993b). Therefore, the observed $n(\sigma)$ does not contain enough systems with small density contrast, and presumably low σ, by definition. The exponential $\Lambda(u)$ partially compensates this underestimate, and the agreement is better.

In any case, the theoretical $n(\sigma)$ confirms that an exponential $\Lambda(u)$ reproduces the data better than the Gaussian $\Lambda(u)$, although not for all the normalizations σ_8. The theoretical $n(\sigma)$ also depends on the power spectrum $P(k)$ (eq. [2.3c]) and on the density of the universe through the perturbation growth factor that enters the Press-Schechter distribution function. Thus, we must interpret the implications of Figure 9 about σ_8 cautiously.

The agreement between curves and observations also depends on the projected separation interval. Marzke et al. (1995) computed $\langle \xi_s(\pi) \rangle$ for the data with the intervals shown in Figure 8. However, the galaxy coordinates in the Zwicky catalog, on which the CfA survey is based, are accurate to $\sim 1'$–$1'.5$. At redshift $cz = 10{,}000$ km s^{-1}, the 3 σ error is thus ~ 0.09–$0.14\ h^{-1}$ Mpc, implying an error in the projected separation ~ 0.13–$0.19\ h^{-1}$ Mpc. With the current data, large errors probably contaminate the interval $[r_{min}, r_{max}] = [0.1, 0.2]\ h^{-1}$ Mpc. Intervals with $r_{min} \geq 0.2\ h^{-1}$ Mpc are more reliable. We also emphasize that galaxy velocities often have uncertainties $\gtrsim 50$ km s^{-1}, which means typical errors $\gtrsim 70$ km s^{-1} in the relative velocities. Thus, we regard the measures of ξ_s at $\pi = 50$, 150 km s^{-1} with caution.

Large differences in χ^2's between the exponential and the Gaussian $\Lambda(u, \sigma)$ (see, for example, Fig. 9 when $\sigma_8 = 0.5$ or

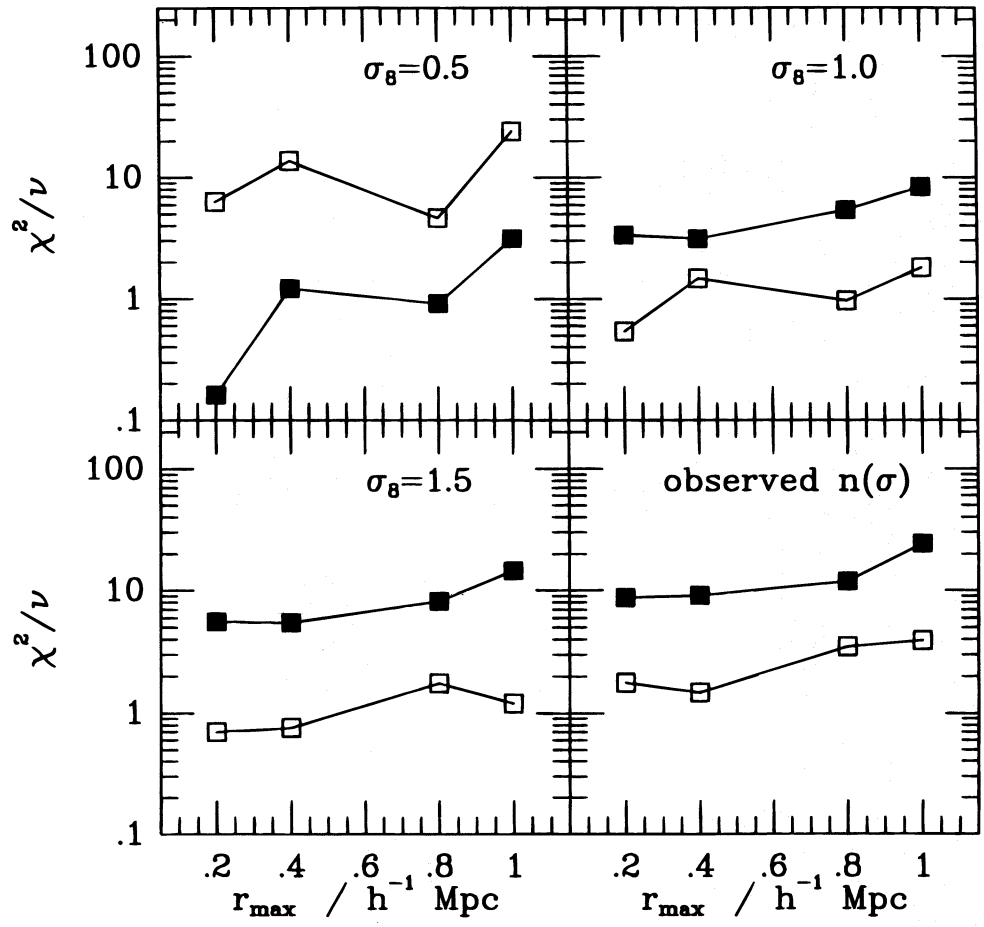

FIG. 9.—Reduced χ^2 with $\nu = 20$ degrees of freedom for the curves in Fig. 8 as a function of the upper limit r_{max} of the integral in eq. (5.2). The four upper limits correspond to the four projected separation intervals $[r_{min}, r_{max}] = [0.1, 0.2]$, $[0.2, 0.4]$, $[0.4, 0.8]$, and $[0.1, 1.0]\ h^{-1}$ Mpc. Open (filled) squares are for an exponential (Gaussian) $\Lambda(u, \sigma)$.

when $\sigma_8 = 1.0$ and $[r_{min}, r_{max}] = [0.1, 0.2]$ or $[0.4, 0.8]$ h^{-1} Mpc) originate mainly at small relative velocities $\pi \lesssim$ 200–300 km s^{-1} (Fig. 8). Thus, by improving the accuracy of galaxy relative positions and velocities by at least a factor of 2, the redshift-space correlation function ξ_s can (1) clearly discriminate among the models and (2) can probably separate the cosmological contribution represented by $n(\sigma)$ from the contribution of the internal dynamics of galaxy systems represented by $\Lambda(u, \sigma)$. Moreover, on very small scales ($r_p \lesssim 0.1$–0.2 h^{-1} Mpc, $\pi \lesssim$ 100–200 km s^{-1}), we expect that the dissipative effects outlined in § 4 will become more apparent. Thus, ξ_s can constrain the importance of mergers in the present universe.

The main conclusion of our analysis is that agreement between the models of the exponential PVDF and the observed redshift-space correlation function on nonlinear scales depends strongly on both the underlying cosmogonic model [namely $n(\sigma)$] and the internal dynamics of galaxy systems [i.e., $\Lambda(u, \sigma)$]. Neither aspect dominates. However, reliable measures of ξ_s at small scales can separate the two contributions and provide further constraints on the model of the universe.

6. CONCLUSION

Marzke et al. (1995) measured the redshift-space correlation function ξ_s for galaxy samples of the Center for Astrophysics (CfA) redshift surveys for galaxy separations $\lesssim 1$ h^{-1} Mpc. An exponential galaxy pairwise velocity distribution function (PVDF) yields the best fit. This result is common to other redshift surveys (see, e.g., Bean et al. 1983; Fisher et al. 1994b).

We propose a physical explanation for this observed exponential shape. If all galaxies belong to isolated galaxy systems with velocity dispersion σ, the PVDF is the weighted sum of the distributions $\Lambda(u, \sigma)$ of the pairwise velocities u within each system. The weight depends on the galaxy number $\nu(\sigma)$ within each system and the number density $n(\sigma)$ of the systems within the sample.

We assume that $\Lambda(u, \sigma)$ is a universal function, identical for each system. This assumption is inadequate, because we show that the shape $\Lambda(u, \sigma)$ depends on the dynamical state of the system. However, if we assume that all the system are virialized, $\Lambda(u)$ is Gaussian and $\nu(\sigma) \propto \sigma^2$. In this case, both the observed $n(\sigma)$ and the $n(\sigma)$ predicted by the Press-Schechter theory in a flat CDM universe yield a nearly exponential PVDF, but only at large relative velocities u. In order to obtain an exponential central peak, $\Lambda(u)$ has to be more centrally peaked than a Gaussian distribution. When a galaxy system is unrelaxed, substructures and infall regions contribute to a centrally peaked $\Lambda(u)$. We limit our analysis to an exponential $\Lambda(u, \sigma)$ that yields the expected central peak of the PVDF. The Gaussian and the exponential distributions represent the two limiting cases. A more detailed analysis of the physical origin of $\Lambda(u, \sigma)$ is likely to yield a $\Lambda(u, \sigma)$ between these two cases. Therefore, we conclude that the observed exponential PVDF testifies to the presence of a large fraction of unrelaxed galaxy systems in the present-day universe.

A third process may increase the frequency of small relative velocities: the transfer of orbital kinetic energy to galaxy internal degrees of freedom. We derive an analytical $\Lambda(u)$ that accounts for energy transfers driven by tidal perturbations. We predict that these perturbations are detectable in galaxy systems with a ratio $\gtrsim 1$ between the internal velocity dispersion of individual galaxies and the velocity dispersion of galaxies within the system. We confirm this prediction by comparing the analytic distribution with N-body simulations and with observed compact groups.

Finally, we compare the measured redshift-space correlation function ξ_s with the convolution of different models of the exponential PVDF with the measured real-space correlation function. The agreement between models and observations depends strongly on both the underlying cosmogonic model and the internal velocity distribution $\Lambda(u, \sigma)$ of galaxy systems. These two effects are of comparable importance over the entire range of relative velocities $\pi < 2000$ km s^{-1}.

We expect to be able to disentangle the two effects with more accurate galaxy coordinate and relative velocity measurements. In fact, the redshift-space correlation function ξ_s at projected separations $r_p \lesssim 0.5$ h^{-1} Mpc and relative velocities $\pi \lesssim 300$ km s^{-1} is very sensitive to the shape of $\Lambda(u, \sigma)$. Thus, a better measure of ξ_s at very small scales poses strong constraints on the shape of $\Lambda(u, \sigma)$ and will improve our understanding of the dynamics of galaxy systems on these scales.

After the submission of this paper, we learned of Sheth's (1996) independent work on the problem of the exponential shape of the PVDF. He investigates a model similar to the model we outline in § 2. He performs an accurate comparison of this model with N-body simulations and shows that for initial density perturbations with power-law power spectra the PVDF is well approximated by an exponential. He shows that the assumptions which underlie our analytic approach in § 2 include the relevant physics.

We sincerely thank Ron Marzke for suggesting the problem of the pairwise velocity distribution and for intensive electronic correspondence. We are grateful to Joe Mohr for providing us with galaxy redshifts of the Abell cluster A576 in advance of publication. We thank Ira Wasserman and Simon White for pointing out some aspects of the internal velocity distributions of galaxy systems that were not adequately treated at an earlier stage, and Bhuvnesh Jain for identifying some initially obscure statements. We thank an anonymous referee for the clarifying suggestions of a prompt report and Ravi Sheth for a careful reading of the manuscript. Invaluable long discussions with Paola Ciarpallini and her inexhaustible support made this work possible. We warmly dedicate this work to Paola. This research is supported in part by NASA grant NAGW-201 and by the Smithsonian Institution. A. D. was a Center for Astrophysics Pre-Doctoral Fellow.

APPENDIX

Here we derive the pairwise velocity difference distributions given in equations (4.1) and (4.2) for dissipative systems. We assume a self-gravitating gas of particles with an initial Gaussian velocity distribution. The particles have internal

degrees of freedom; tidal effects increase the particle internal energy during particle motion within the system at the expense of the orbital kinetic energy of the particles. In the following derivation, we ignore particle mass loss, and therefore we underestimate the total kinetic energy loss as discussed in § 4.

First, we compute the fraction of the relative kinetic energy transferred into the particle internal degrees of freedom. We then derive an approximated pairwise velocity difference distribution.

Suppose that the particles have equal mass m. E is the relative kinetic energy per unit mass of two particles in their center-of-mass reference frame. If v is their relative velocity, we have $E = v^2/4 = \sigma_s^2 u^2/2$, where σ_s is the one-dimensional velocity dispersion of the system and $u = v/2^{1/2}\sigma_s$.

Spitzer (1958) considered the encounter between a cloud and a star cluster and computed the relative energy transfer to the internal energy of the cluster during the encounter. The derivation is similar to the derivation of the energy transfer in a Coulomb collision between a moving charge and a harmonically bound charge in the dipole approximation (Jackson 1962). In fact, Spitzer assumed that for the stars in the cluster (1) the tidal force of the cloud is small compared with the gravitational attraction of the cluster and (2) the internal gravitational potential of the cluster is proportional to the square of the distance from the cluster center, i.e., the stars are harmonic oscillators with the same frequency.

In Spitzer's paper, the cloud and cluster have mass m_n and m_c, respectively; r_c^2 is the mean square cluster radius; $1/\omega$ the oscillation period of the stars in the cluster, v is the cloud-cluster relative velocity; and p is the impact parameter. Spitzer showed that the increase of the cluster internal energy after a single encounter is

$$\Delta E = \frac{m_c r_c^2}{6}\left(\frac{2Gm_n}{vp^2}\right)^2 L\left(\frac{2\omega p}{v}\right), \tag{A1a}$$

where G is the gravitational constant and

$$L(\theta) = 2\theta^2[\theta^2 K_0^2(\theta) + \theta K_0(\theta)K_1(\theta) + (1+\theta^2)K_1^2(\theta)], \tag{A1b}$$

where K_0 and K_1 are the usual modified Bessel functions, and $\theta = 2\omega p/v$.

When $v \to \infty$, $L(\theta) \to 2(1 + 2\theta^2) \to 2$, and equation (A1a) reduces to the usual impulse approximation. When $v \to 0$, $L(\theta)/v^2 \to \pi\theta^3 \exp(-2\theta)/v^2 \to 0$; the energy loss falls exponentially to zero. Weinberg (1994a, 1994b, 1994c) shows that such an adiabatic cutoff is not correct in general. In fact, ΔE approaches zero when $\omega/v \to \infty$. However, a stellar system always has stars with arbitrary small ω, and for those stars we never have $\omega/v \to \infty$. The perturbation suffered by those stars ultimately affects the internal dynamics of the whole stellar system. Thus, assuming $\Delta E \sim 0$ when $v \to 0$ will underestimate the energy loss. However, we would detect such energy loss only on timescales $\gtrsim R/v$, where R is some characteristic size of the system. In other words, we underestimate the energy loss only if we observe the system for a sufficiently long time interval.

We apply equations (A1) to galaxy systems in which the adiabatic approximation does not break down because we do not observe them for a long enough time. In fact, either galaxy systems are dynamically young because they suffer a merging instability and are therefore intrinsically unstable (groups) or their size is large enough that when v is small, R/v is greater than the Hubble time (clusters). Therefore, we expect that equations (A1) approximate the energy loss for galaxies within groups and clusters.

Let us now apply equations (A1) to a system of equal mass galaxies. All possible galaxy pair combinations reduce to a "reduced" galaxy with mass $m_n = m/2$ (the "cloud"), which moves with velocity v through a field of fixed sources with mass $m_c = 2m$ (the "clusters"). The "cloud" loses a fraction of its kinetic energy at a rate given by ΔE times the number of collisions per unit time, integrated over the impact parameter p and the mass of the "clusters" m_c. In other words, if $n(m_c)$ is the number density of "clusters" with mass between m_c and $m_c + dm_c$, we have

$$\frac{dE}{dt} = -\int \Delta E \times v \times 2\pi p\, dp \times n(m_c)dm_c = v \times \frac{m_n^2 r_c^2}{6}\left(\frac{2G}{v}\right)^2 2\pi\left(\frac{2\omega}{v}\right)^2 \int_{\theta_{\min}}^{\infty} \frac{L(\theta)}{\theta^3}\, d\theta \int m_c\, n(m_c)dm_c\,. \tag{A2a}$$

We assume that all the "clusters" have the same mass $m_c = 2m$. Thus, the "cluster" mass spectrum per unit volume is $n(m_c) = n_0\,\delta(2m - m_c)$, where δ is the usual Dirac delta function.

The quantity $\theta_{\min}$ depends on the validity of assumption (1) above, namely that the "cloud" exerts a tidal force on a "cluster" star which is small compared to the "cluster" attraction. We can write

$$\theta_{\min} = \frac{2\omega p_{\min}}{\sqrt{2}\,\sigma_s u} \equiv \frac{\varphi}{u}\,. \tag{A3}$$

The oscillation period $1/\omega$ of the star within the "cluster" is roughly twice the inverse of the crossing time $r_c/3^{1/2}\sigma_i$, where σ_i is the one-dimensional velocity dispersion within the "cluster." Therefore

$$\varphi = \frac{\sqrt{6}}{2}\left(\frac{\sigma_i}{\sigma_s}\right)\frac{p_{\min}}{r_c}\,. \tag{A4}$$

For $p_{\min} \sim r_c$ and $\sigma_i \sim \sigma_s$ we expect $\varphi = 6^{1/2}/2 \sim 1.22$.

Applying the recursion formulas $dK_0/d\theta = -K_1$ and $dK_1/d\theta = -K_0 - K_1/\theta$, the indefinite integral over θ is

$$-\int \frac{L(\theta)}{\theta^3}\, d\theta = 2\theta K_0(\theta)K_1(\theta) + K_1^2(\theta) \equiv \tilde{L}(\theta)\,. \tag{A5}$$

Finally, equation (A2a) reduces to

$$\frac{dE}{dt} = -\frac{8\pi}{3} m r_c^2 n_0 \omega^2 (Gm)^2 \frac{1}{v^3} \tilde{L}\left(\frac{\varphi}{u}\right). \tag{A2b}$$

For the virial theorem $Gm = 3\sigma_i^2 r_c$. Moreover, $\omega = 3^{1/2}\sigma_i/2r_c$ and $n_0 = 3N/4\pi R_s^3$, where R_s is the size of the system and N is the total number of galaxies within the system. We can write $N = GfM_{\rm tot}/Gm = f(\sigma_s/\sigma_i)^2(R_s/r_c)$, where $fM_{\rm tot}$ is the fraction of the total mass concentrated in galaxies. The crossing time of the system is $t_{\rm cr} = 3^{1/2}\sigma_s/R_s$; thus, we have

$$\frac{dE}{dt} = -\frac{m\sigma_s^2}{t_{\rm cr}} \frac{9\sqrt{6}}{8} N \left(\frac{\sigma_i}{\sigma_s}\right)^6 \left(\frac{r_c}{R_s}\right)^2 \frac{1}{u^3} \tilde{L}\left(\frac{\varphi}{u}\right) = -\frac{m\sigma_s^2}{t_{\rm cr}} \frac{9\sqrt{6}}{8} f \left(\frac{\sigma_i}{\sigma_s}\right)^4 \left(\frac{r_c}{R_s}\right) \frac{1}{u^3} \tilde{L}\left(\frac{\varphi}{u}\right) \equiv -\frac{m\sigma_s^2}{t_{\rm cr}} \beta \frac{1}{u^3} \tilde{L}\left(\frac{\varphi}{u}\right), \tag{A2c}$$

where we have introduced the constant

$$\beta = \frac{9\sqrt{6}}{8} f \left(\frac{\sigma_i}{\sigma_s}\right)^4 \left(\frac{r_c}{R_s}\right). \tag{A2d}$$

The constant β contains information about the size and the internal velocity dispersion of galaxies compared with those of the whole system. It is apparent that the energy transfers into galaxy internal degrees of freedom is mainly sensitive to the ratio of the velocity dispersions. The constant β specifies when we can ignore the galaxy internal degrees of freedom. We see that within galaxy groups, the energy transfer must be more clearly detectable than in galaxy clusters.

The energy transfer rate per unit mass in unit of σ_s^2 may finally be written

$$\frac{dE}{dt} = -\frac{1}{t_{\rm cr}} \beta \frac{1}{u^3} \tilde{L}\left(\frac{\varphi}{u}\right). \tag{A6}$$

Suppose now that we know the relative kinetic energy distribution $q(E)dE$ at time t. We wish to compute the energy distribution $\lambda(E)dE$ at time $t + \eta t_{\rm cr}$, when $\eta \to 0$, so that $u \sim$ const.

Using equation (A6), the relative kinetic energy per unit mass in unit σ_s^2 at the time $t + \eta t_{\rm cr}$ is, to first order in η,

$$E(t + \eta t_{\rm cr}) = E(t) + \frac{dE}{dt} \eta t_{\rm cr} = E(t) - \eta\beta\,\Delta(u, \varphi), \tag{A7a}$$

where

$$\Delta(u, \varphi) = \frac{1}{u^3} \tilde{L}\left(\frac{\varphi}{u}\right). \tag{A7b}$$

Now, the probability density $\lambda(E)dE$ is

$$\lambda(E)dE = q[G^{-1}(E)] \frac{dG^{-1}(E)}{dE} dE, \tag{A8}$$

where the inverse function G^{-1} is defined through equations (A7):

$$E = G(E_0) = E_0 - \eta\beta\,\Delta(E_0) \tag{A7c}$$

and $E(t) = E_0$.

In the limit $\eta \to 0$, we have to first order in η

$$G^{-1}(E) = E + \eta\beta\,\Delta(E), \tag{A9}$$

and we may rewrite equation (A8)

$$\lambda(E)dE = q(E)\left[1 + \eta\beta\,\Delta(E)\left\{\frac{d\ln[q(E)]}{dE} + \frac{d\ln[\Delta(E)]}{dE}\right\}\right]dE. \tag{A10}$$

Equation (A10) is valid only when $\eta \to 0$, i.e., for times close to t when the distribution $q(E)$ is known. We should obtain the distributions $\lambda(E, t)dE$ at different times t by solving the correct Boltzmann equation specific for our problem. However, we wish to have an analytic distribution to compare with real systems. Therefore, we go further and use equation (A10) tout court assuming $\alpha = \eta\beta$ is a free-fit parameter. We justify this assumption with the following argument: if $q(E) = \lambda_0(E)$ at time t_0 and $\lambda(E) = \lambda_1(E)$ at time t_1, we again have equation (A10) at time t_2, where $q(E) \to \lambda_1(E)$ and $\lambda(E) \to \lambda_2(E)$. To first order in η, $\eta\beta \to 2\eta\beta$. Thus, if we apply this iterative procedure, the form of equation (A10) does not change, but now the coefficient α tells us how far the system is dynamically from the initial distribution $q(E)$. Moreover, the coefficient α is a measure (1) of the timescale of the relative velocity change because of kinetic energy loss (η) and (2) of the similarity of the galaxy internal dynamics to the galaxy system dynamics (β).

If we assume a Maxwellian $q(E)$

$$q(E)dE \propto E^{1/2}e^{-E}\,dE\,, \tag{A11}$$

equation (A10) becomes, in terms of the velocity modulus $u = v/2^{1/2}\sigma_s = (2E)^{1/2}$ and with the explicit expression of $\Delta(u)$ (eq. [A7b]),

$$\lambda(u)du \propto u^2 \exp\left(-\frac{u^2}{2}\right)[1 - \alpha H(u, \varphi)]du\,, \tag{A12a}$$

where

$$H(u, \varphi) = \frac{1}{u^3}\tilde{L}\left(\frac{\varphi}{u}\right)\left\{1 + \frac{2}{u^2} + \frac{\varphi}{u^3}\frac{d\ln[\tilde{L}(\theta)]}{d\theta}\right\}. \tag{A12b}$$

The one-component velocity density distribution $\Lambda(u)du$ is related to the density distribution of the velocity moduli through the equation (Feller 1966)

$$\lambda(u)du = -u\frac{d\Lambda(u)}{du}\,. \tag{A13}$$

Equation (A13) holds for any isotropic three-dimensional random field. With the boundary condition $\Lambda(u) \to 0$ when $u \to \infty$, we obtain

$$\Lambda(u)du \propto \int_u^\infty \frac{\lambda(t)}{t}\,dt\,. \tag{A14}$$

In other words,

$$\Lambda(u)du \propto \exp\left(-\frac{u^2}{2}\right)[1 - \alpha\tilde{H}(u, \varphi)]du\,, \tag{A15a}$$

where

$$\tilde{H}(u, \varphi) = \exp\left(\frac{u^2}{2}\right)\int_u^\infty t\exp\left(-\frac{t^2}{2}\right)H(t, \varphi)dt\,. \tag{A15b}$$

REFERENCES

Bean, A. J., Efstathiou, G., Ellis, R. S., Peterson, B. A., & Shanks, T. 1983, MNRAS, 205, 605
Bond, J. R., Cole, S., Efstathiou, G., & Kaiser, N. 1991, ApJ, 379, 440
Bower, R. J. 1991, MNRAS, 248, 332
Bunn, E. F., Scott, D., & White, M. 1995, ApJ, 441, L9
Carlberg, R. G. 1994, ApJ, 433, 468
Castaing, B., Gagne, Y., & Hopfinger, E. J. 1990, Physica D, 46, 177
Catelan, P., & Scherrer, R. J. 1995, ApJ, 445, 1
Cen, R., & Ostriker, J. P. 1993, ApJ, 417, 415
Cole, S. M., & Lacey, C. G. 1996, MNRAS, in press
Colless, M., & Dunn, A. M. 1996, ApJ, 458, 435
Couchman, H. M. P., & Carlberg, R. G. 1992, ApJ, 389, 453
Crone, M. M., Evrard, A. E., & Richstone, D. O. 1994, ApJ, 434, 402
Crone, M. M., & Geller, M. J. 1995, AJ, 110, 21
Davis, M., Efstathiou, G., Frenk, C. S., & White, S. D. M. 1985, ApJ, 292, 371
Davis, M., & Peebles, P. J. E. 1983, ApJ, 267, 465
Diaferio, A., Geller, M. J., & Ramella, M. 1994, AJ, 107, 868
———. 1995, AJ, 109, 2293
Diaferio, A., Ramella, M., Geller, M. J., & Ferrari, A. 1993, AJ, 105, 2035
Doe, S. M., Ledlow, M. J., Burns, J. O., & White, R. A. 1995, AJ, 110, 46
Efstathiou, G. P., Frenk, C. S., White, S. D. M., & Davis, M. 1988, MNRAS, 235, 715
Evrard, A. E., Mohr, J. J., Fabricant, D. G., & Geller, M. J. 1993, ApJ, 419, L9
Evrard, A. E., Summers, F. J., & Davis, M. 1994, ApJ, 422, 11
Feller, W. 1966, An Introduction to Probability Theory and Its Application, Vol. II (New York: John Wiley & Sons)
Fisher, K. B. 1995, ApJ, 448, 494
Fisher, K. B., Davis, M., Strauss, M. A., Yahil, A., & Huchra, J. P. 1994a, MNRAS, 266, 50
———. 1994b, MNRAS, 267, 927
Frenk, C. S., Evrard, A. E., White, S. D. M., & Summers, F. J. 1996, ApJ, submitted
Fusco-Femiano, R., & Menci, N. 1995, ApJ, 449 431
Gelb, J. M., & Bertschinger, E. 1994, ApJ, 436, 491
Geller, M. J., & Peebles, P. J. E. 1973, ApJ, 184, 329
Gunn, J. E., & Gott, J. R. 1972, ApJ, 176, 1
Hernquist, L. 1987, ApJS, 64, 715
Hernquist, L., Katz, N., & Weinberg, D. H. 1995, ApJ, 442, 57
Hickson, P. 1993, Ap. Lett. Comm., 29, 1
Ida, S., & Taguchi, Y.-H. 1996, ApJ, submitted
Jackson, J. D. 1962, Classical Electrodynamics (New York: John Wiley & Sons)
Jing, Y. P., & Fang, L. Z. 1994, ApJ, 432, 438
Jing, Y. P., Mo, H. J., Börner, G., & Fang, L. Z. 1995, MNRAS, 276, 417
Kauffmann, G., & White, S. D. M. 1993, MNRAS, 261, 921
King, I. R. 1965, AJ, 70, 376
———. 1966, AJ, 71, 64
Kofman, L., Bertschinger, E., Gelb, J. M., Nusser, A., & Dekel, A. 1994, ApJ, 420, 44
Lacey, C. G., & Cole, S. M. 1993, MNRAS, 262, 627
———. 1994, MNRAS, 271, 676
Lynden-Bell, D. 1967, MNRAS, 136, 101
Mamon, G. A. 1992a, in Distribution of Matter in the Universe, ed. G. A. Mamon & D. Gerbal (Paris: Observatoire de Paris), 51
———. 1992b, in ASP Conf. Ser. 70, Groups of Galaxies, ed. O. G. Richter & K. Borne (San Francisco ASP), 173
Marzke, R. O., Geller, M. J., Da Costa, N. L., & Huchra, J. P. 1995, AJ, 110, 477
Mazure, A., et al. 1996, A&A, in press
Miesch, M. S., & Scalo, J. M. 1995, ApJ, 450, L27
Mohr, J. J., Fabricant, D. G., Geller, M. J., Wegner, G., Thorstensen, J., & Richstone, D. O. 1996, ApJ, in press
Narayan, R., & White, S. D. M. 1988, MNRAS, 231, 97P
Navarro, J. F., Frenk, C. S., & White, S. D. M. 1996, ApJ, 462, 563
Nusser, A., Dekel, A., & Yahil, A. 1995, ApJ, 449, 439
Padmanabhan, T. 1990, Phys. Rep., 188, 285
Peebles, P. J. E. 1976, Ap&SS, 45, 3
Press, W. H., & Schechter, P. 1974, ApJ, 187, 425

Ramella, M., Diaferio, A., Geller, M. J., & Huchra, J. P. 1994, AJ, 107, 1623
She, Z.-S. 1991, Fluid Dyn. Res., 8, 143
Sheth, R. K. 1996, MNRAS, 279, 1310
Shu, F. H. 1978, ApJ, 225, 83
Spitzer, L. 1958, ApJ, 127, 17
van der Marel, R. P., & Franx, M. 1993, ApJ, 407, 525
Weil, M. L., & Hernquist, L. 1996, ApJ, 460, 101
Weinberg, M. D. 1994a, AJ, 108, 1398
———. 1994b, AJ, 108, 1403
———. 1994c, AJ, 108, 1414
West, M. J., Jones, C., & Foreman, W. 1995, ApJ, 451, L5
White, S. D. M. 1996, in Cosmology and Large-Scale Structure, ed. R. Schaeffer, J. Silk, & J. Zinn-Justin (Dordrecht: Elsevier), in press
White, S. D. M., & Frenk, C. S. 1991, ApJ, 379, 52
Zabludoff, A. I., Franx, M., & Geller, M. J. 1993a, ApJ, 419, 47
Zabludoff, A. I., Geller, M. J., Huchra, J. P., & Ramella, M. 1993b, AJ, 106, 1301
Zurek, W. H., Quinn, P. J., Salmon, J. K., & Warren, M. S. 1994, ApJ, 431, 559